Renewable and Sustainable Energy Reviews 238 (2026) 117066

Contents lists available at ScienceDirect

Renewable and Sustainable Energy Reviews

journal homepage: www.elsevier.com/locate/rser

Recent advancement and prospects of graphite nanocomposites as anode materials for lithium-ion batteries

Ntalane Sello Seroka [a,*], Mmalewane Modibedi [a], Haitao Zheng [a,**], Lindiwe Khotseng [b], Hongze Luo [a]

[a] Energy Centre, Smart Places Cluster, Council for Scientific and Industrial Research (CSIR), Pretoria, 0001, South Africa
[b] Department of Chemistry, University of the Western Cape, Robert Sobukwe Rd, Private Bag X17, Bellville, 7535, South Africa

ARTICLE INFO

Keywords:
Sustainable energy storage
Graphite nanocomposites
Reaction kinetics
Battery technology
Innovative materials

ABSTRACT

Rechargeable batteries in the energy storage sector are seen as both current and future critical energy production and storage technologies. They are essential in the day-to-day of hybrid and electric vehicles, given their reliable sustainability and performance metrics amongst energy storage technologies. The pertinent challenges such as flammable electrolytes, safety concerns, costs, and environmental recovery impede their widespread adoption in energy storage efficiency, i.e lithium-ion batteries. This study gives key insights on lithium-ion batteries that are not limited to reaction mechanisms, storage mechanisms, material development, structural features, and preservation. Provides key aspects in optimal solid electrolyte interfaces and graphite intercalation compounds; investigates innovative materials such as biochar, as well as their composites with graphite. The review delves into reaction mechanics and kinetics in rechargeable batteries and current trends in the advancement of these technologies. Lithium-ion storage in graphite, and nanocomposites with factors influencing oxygen defects, interlayer spacing, and stacking attributes. These structural and morphological properties affect the diffusion pathways within the expansive framework pores of lithium ion, these defects, and in addition improve the surface area. The structural, morphological, and textural and their synergistic effects on the overall performance metrics are also discussed in the paper.

1. Introduction

The global energy crisis is intensifying, leading to increased research and development in clean energy technologies. As a result, there is growing focus on energy storage and conversion technologies, particularly within the lithium-ion battery (LIB) industries. Since its commercialisation in the 1990s, lithium-ion technology has been extensively investigated, mainly due to its use of stable graphite anode materials that provide significant lithium intercalation storage capabilities. The anode material that leads the market share for lithium-ion batteries is graphite. The reliability, sustainability and abundance of graphite which promotes the large-scale production of lithium-ion technology has been intensively studied over the years due to its electrochemical stability and tunable structure with a specific capacity of 372 $mAhg^{-1}$ [1].

The hard and soft carbon were later replaced by graphite with the development of a lithium-ion battery. The capacity discharge of graphite (0.2 V vs Li+/Li), and several disadvantages, one of them being that it has very limited capacity, especially when the battery is charging due to exfoliation. This is mainly because storage of lithium ions in graphite pores is reduced, leading to parasitic reactions during charging and discharging. These reactions, combined with an ohm overpotential, result in decreased capacity because of the large pores and short diffusion pathways. The interface between the graphite surface and the solid electrolyte interface (SEI) can address the issues, particularly when the SEI is thin and demonstrate low or negligible resistance. With the advancement of nanotechnology, graphite can be tailored to possess specific physical, chemical, mechanical, and electrical properties. These improvements open new avenues for the development of advanced energy storage materials [2,3].

Graphite is approximately 98% of the market share for anode materials in lithium-ion batteries with around 2% attributed to $Li_4Ti_5O_{12}$ (LTO) anodes. Its dominance is due to unique advantages such as abundant availability, low-cost, high-energy density at low cycling potentials, strong power density and exceptionally long cycle life -making

* Corresponding author.
** Corresponding author.
E-mail address: nseroka@csir.co.za (N.S. Seroka).

https://doi.org/10.1016/j.rser.2026.117066
Received 12 January 2026; Received in revised form 19 March 2026; Accepted 29 April 2026

graphite anode highly competitive. Although high-capacity alternatives such as silicon (Si), silicon oxides (SiO_x), lithium metal, sulphides and various oxides are actively being researched, only a few have shown the potential to rival graphite in overall performance and commercial viability of LIBs [4,5].

Because LIBs are an environmentally friendly battery technology, their production and usage are set for continuous growth to maintain a more sustainable zero-emission infrastructure for their application, as shown in Fig. 1a. That being said and the less effect they present towards global warming and climate change, they are considered a substitute for fossil fuels in energy storage, but despite that they also show their own environmental challenges such as the 34−77 kg CO_2 kWh^{-1} estimate of carbon dioxide that is released into the environment from source to production of LIBs, which was estimated using life cycle assessment (LCA) data. For the worldwide growth and adoption of LIBs, production is a very important aspect to consider. The LIBs, which are on the ongoing trend, are made of four main components that can be distinguished by weight: cathode and (~41%), anode (~41%), separator (~3%) and electrolyte (~15), as shown in Fig. 1c below [6,7].

The anode is a crucial component of the LIB, as it acts as a host of Li^+ in the charged state, so the type of material used is of essential importance. Among the different anode materials, graphite has been found to be the best choice due to its stable theoretical capacity (372 $mAhg^{-1}$), high Li^+ diffusion coefficient (~10−11 cm^2 s^{-1}) and the delithiation potential (0.02–0.2 V vs. Li/Li^+), since its initial use, and has maintained its position as the anode material of choice, which is used in nearly all LIBs currently sold in the market. The cathode on the other side consists of continuously changing materials depending on the specific demand, changing from LiCoO2 to LiNixMnyCozO2 to LiFePO4, as demonstrated in Fig. 1b. Nevertheless, different types of anode material have been widely researched, and graphite remains dominant and unchallenged. It is predicted that in the future it will remain as is because of its technological maturity and exceptional electrochemical performance. The European Critical Raw Materials Act and the UK government have listed graphite as one of the 17 strategic critical raw materials and has been defined as a mineral of high crucial importance in the modern world. Then it is crucial to reconsider and improve the production of graphite from both both environmental and economic sustainability point of view while improving the eco-friendly effect of LIBs on the environment that supports the goals of sustainable development [6–8].

The electrochemistry of graphite still needs further studies to improve the commercial application of LIBs in grid-scale energy storage and electric vehicles. The storage mechanism of Li in the graphite anode is mostly attributed to intercalation and de-intercalation between graphite layers, forming a series of graphite intercalation compounds (GICs). However, there remains a lack of a comprehensive understanding of the storage mechanisms and performance limitations. It is widely believed that there has been a limited adoption of LIBs with high-rate performance-particularly under the fast charging conditions of graphite. To address issues such as Li dendrite formation and associated safety concerns, the development of graphite-based nanocomposites is urgently desired for next-generation energy storage systems and electric vehicles [8,9].

Intercalation electrodes function by topotactical incorporating lithium ions (Li^+) into their crystal lattice. To maximise cell capacity, these electrodes must enable sustainable lithium insertion and extraction while maintaining high electronic and ion conductivity to reduce polarization. In achieving high power densities and high current, this is pivotal, especially when safety issues are highly linked to lithium metal. In quest of achieving reversible lithium intercalation properties, carbon-based materials have shown great potential. With graphite being the most used anode material due to its excellent and ease of intercalating property with many materials, approximately 1 mol of lithium ions per mole of carbon is twice the capacity of coke. The intercalating property, combined with diffusivity of lithium ions and reversibility, cycling stability, cost-effectiveness, and abundance makes it dominate the market share. With carbon allotropes, graphite remains the widely adopted anode electrode material and is facing a commercial reality [8–11].

Graphite is a 2D nanomaterial, a commonly known allotrope of carbon, possessing multilayers held together by weakly bound van der Waals forces. Graphene is a single-layer graphite with a hexagonal packed lattice. When high pressure is applied, the interlayer bonding weakly bound promotes the distortion, for example when a pencil leaves traces on paper due to bond breakage induced by frictional forces. Studies have reported that a micrometre section of graphite has approximately 3 million sheets. Thus, a single atomic layer of carbon, assuming the honeycomb structure, is known as graphene. Graphene is regarded as an unrolled single-walled nanotube (SWNT) that has a larger surface area. Graphene has outstanding electrical conductivity, a high surface-to-volume ratio, an ultra-thin thickness, an exceptional porous structure, a high structural flexibility, and chemical stability. Therefore, graphite has attracted the attention of researchers as a new and effective electrode material in LIBs. The 3D (diamond) tetrahedral lattice, graphite a layered hexagonal lattice, monolayer graphene, fullerenes 0D closed cage or 1D tubular structures are carbon allotropes. Studies show that stacking of layers forms a 3D crystalline structure of graphite, observed from graphene. The graphitic domains in various dimensions can be configured as 0D fullerenes, 1D nanotubes, and or 3D graphite.

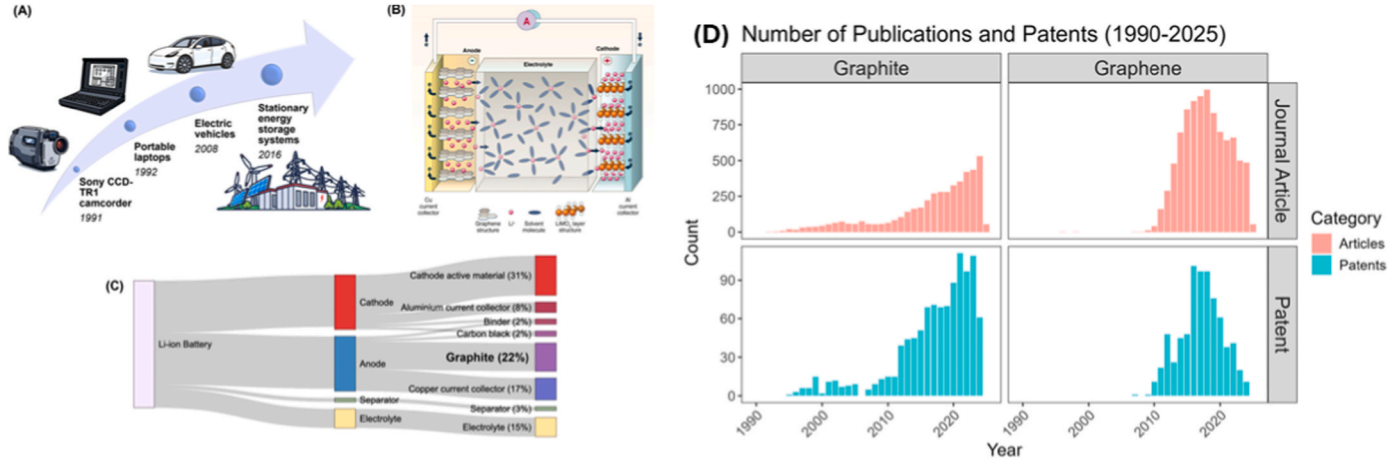

Fig. 1. Illustrating the (**a**) trend of LIBs production from 1990s, (**b**) materials which makes up a LIB, (**c**) main components of LIBs distinguished using weight, and (**d**) number of publications and patents right from the 1990s until 2025. Reproduced with permission from Ref. [8], © 2025 The Authors, John Wiley & Sons Australia, Ltd.

The sp^2 hybridized carbon covalently bonded to 3 adjacent carbons in a single layer graphite known as graphene leads to structural stability. The conduction plane is induced through pi and pi* carbon bonds with the remaining 2p orbital in a perpendicular direction [12–16].

LIBs with high energy density demand are poised to improve the performance of graphite using compositing methodology. To meet this requirement, graphite impregnation with nanostructured materials can be an effective strategy to enhance its theoretical capacity. In the nanoscale range, it is easier to tailor the properties of the materials and effectively increase their surface area promoting a wider active site with the electrolyte. The huge contact area allows for the large number of lithium-ion mobility at the electrolyte electrode interface, hence increasing the capacity thereof. Nanostructured materials often lead to desirable reactions such as increased interactions at the electrode surface that simply cannot be possible in bulk in materials. In the quest to meet global energy demands, LIBs graphite-based anodes offer key benefits such as durability, high-rate capability, increased capacity and cycling stability. To fully maximise the advanced storage avenues of graphite nanocomposites, research and innovative strategies are essential in harnessing the synergy and morphology of graphite nanocomposites which contributes significantly to the lithium storage and electrochemical properties [15,16].

In this study we investigate the importance of graphite nanocomposites as anode material in LIBs as well as biochar nanocomposites. The effective strategies to improve the capacity and energy density, nanomaterials, chemical and physical properties and how they affect the overall performance of LIBs.

2. Fundamental reaction mechanisms of graphite anodes

Graphite anode materials remain dominant in the market share, ideal for lithium-ion systems given its relatively low lithiation potential of ~0.1 V vs Li/Li^+, high theoretical capacity of 372 mAh g^{-1} for LiC_6 and its remarkable structural stability. The structural principles governing ion storage involves the reversible intercalation of Li ions between the layers resulting in staged graphite intercalation compounds (GICS). These processes involve the ion transport in electrolyte media, desolvation at the electrode/electrolyte interface, transportation across the SEI, charge transfer at the graphite surface, diffusion of solid state within graphite galleries, and phase changes within the staging structures. The processes largely determine the overall intercalation kinetics and rate capability of graphite anodes, and recent work clearly reports on interfacial processes rather than bulk diffusion more often dominates the kinetic limitation in fast charging systems [17,18].

2.1. Li^+ intercalation kinetics

The graphite lithiation process is a multistep kinetic pathway (1) which can be explained by a combination of interfacial and bulk processes.

$$\boldsymbol{Li^+_{sol} \rightarrow Li^+_{desol} \rightarrow Li^+_{SEI} \rightarrow Li^+_{ads} \rightarrow Li_xC_6} \quad (1)$$

The first process involves Li^+ desolvation at the electrolyte interface where Li^+ ions must shed their solvation shell near the inner Helmholtz plane. This involves the breaking of Li^+ -solvent coordination bonds, and activation energy to promote intercalation. The electrolyte composition is a crucial factor in this step due to the solvation structure, and the binding energy of Li^+ complexes. Subsequently, Li^+ transport across the SEI after desolvation demand diffusion through the SEI layer formed on graphite. This can happen given the SEI composition, ionic conductivity, thickness and morphology. These are key factors which show ensures rapid Li^+ diffusion in SEI. Researchers reported that LiF rich or inorganic SEI phases are suitable for agile Li^+ transport thereby reducing the interfacial resistance and thus enhanced fast charging capability [17–19]. The charge transfer and surface adsorption can be seen through the reaction (2) below:

$$\boldsymbol{Li^+ + e^- \rightarrow Li_{ads}} \quad (2)$$

The electron transfer takes place at the graphite surface, edge sites or defect sites. The edge planes are more reactive than basal planes because of high electronic density, open lattice structure. Therefore, the engineered graphite has the potential to facilitate earlier electrolyte decomposition and controlled SEI formation. The 4th step would be solid state diffusion and staging transition, where Li^+ diffuses between the graphite galleries producing staged compounds; stage IV → III → II → I (LiC_6), after insertion into graphite layers. The phase transition with moving phase boundaries where lithiation phase is involved adheres to rather than simple diffusion in a homogenous solid. The incomplete lithiation at high current densities and subsurface lithium accumulation during fast charging it is noteworthy the coexistence of multiple staging mechanisms. Lastly the rate determining step depends on electrode conditions. The dominant kinetic limitations for instance are thin particles and high C-rate when interfacial Li diffusion process takes place. For particle size smaller than ~10 μm the interfacial diffusion through the SEI becomes the primary rate limiting step, because thick SEI or unstable electrolyte is predominant during SEI transport. Moreover, large particle size, thick electrodes are kinetic limitations during solid diffusion in graphite and electrode transport, respectively [19].

2.1.1. SEI formation thermodynamics and kinetics

The SEI is a fundamental component and one of the key determinants of overall battery performance. Its thermodynamic formation begins when the operating potential of graphite falls below the reduction potentials of the electrolyte constituents. The reduction reactions that generate this passivating layer yield a mixture of inorganic and organic species, including Li_2CO_3, LiF, Li_2O, $ROCO_2Li$, and polymeric carbonates. Consequently, SEI formation primarily takes place during the initial charge–discharge cycles, as the graphite surface becomes stabilized. In most cases, SEI growth is thermodynamically favored because the electrolyte's operating potential window collapses spontaneously once the electrode potential drops below the electrolyte's LUMO level, Fig. 2a–c. Since the reactions that control intercalation kinetics are closely linked to SEI behaviour, this interphase impacts graphite performance by introducing interfacial resistance, which Li^+ ions must traverse before intercalating into the graphite [20].

$$\boldsymbol{EC + e^- + Li^+ \rightarrow Li_2CO_3 + ROCO_2Li} \quad (3)$$

$$\boldsymbol{R_{SEI} \propto \frac{L}{\sigma Li}} \quad (4)$$

Where in (4), (L) denotes SEI thickness and (σ_{Li}) denotes ionic conductivity.

SEI growth influences the overall reaction kinetics through several interconnected processes: electrons must tunnel through an ever-thickening SEI formed by electrolyte reduction at the interface, Li^+ ions diffuse across SEI components and products, and decomposition species precipitate out of the SEI. Together, these processes reduce the initial capacity via a classical self-limiting growth mechanism and diminished electron transport caused by the increasing SEI thickness, which in turn makes Li^+ migration progressively more difficult. As a result, reduction reactions slow down and the SEI eventually reaches a quasi-stable state. Nevertheless, the SEI remains dynamic and continues to evolve during cycling [21].

Structurally, the SEI is generally described as a bilayer: the inner layer consists predominantly of inorganic species such as LiF, Li_2O, and Li_2CO_3, which provide good mechanical strength and support Li^+ conduction. The outer SEI is richer in organic, polymeric carbonate species, giving it a more porous, electrolyte-permeable character. An SEI enriched in inorganic components is typically preferred, as it offers superior Li^+ transport and enhanced stability.

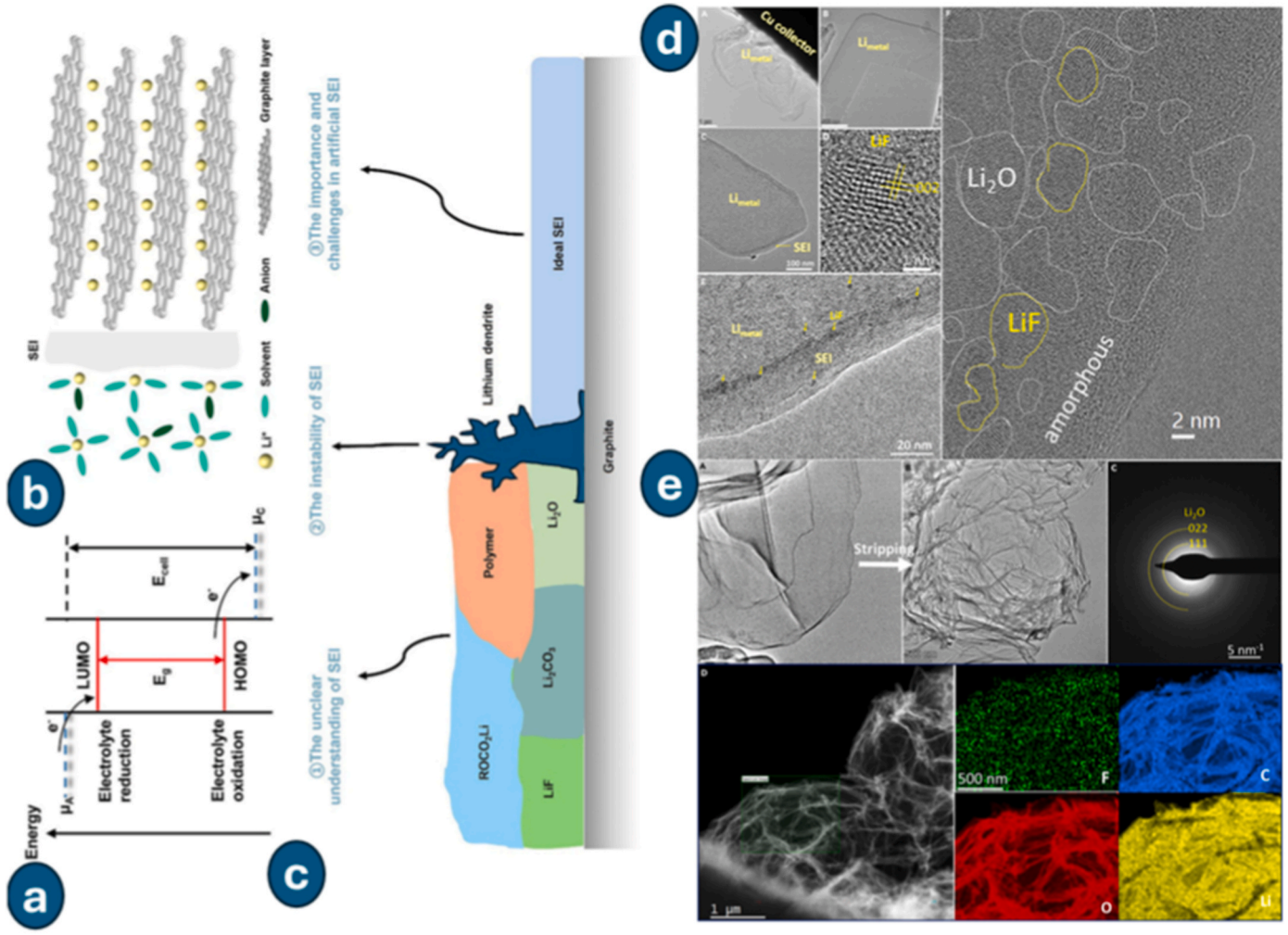

Fig. 2. Schematic illustration of (a) SEI formation at both electrode interfaces, (b) SEI development on graphite during cycling, and (c) the main SEI-related challenges [40]. (d) Cryo-TEM and (e) Cryo-TEM combined with electron diffraction and cryo-STEM/EELS mapping [41].

Recent SEI engineering strategies aim to mitigate sluggish Li^+ transport and poor intercalation through the SEI, issues that often trigger lithium plating on graphite anodes, thereby raising safety risks and accelerating cell degradation. In this context, Li_3P-based SEI layers have been shown to support fast charging rates of 6–10 C by tailoring SEI composition and enabling rapid reaction kinetics via improved Li^+ diffusion. Additionally, edge-engineered graphite promotes early anion decomposition and the formation of a LiF-rich SEI, which helps suppress lithium plating and lowers the Li^+ desolvation barrier [18–22].

2.2. Graphite nanocomposites in lithium-ion batteries

Graphite is a carbon source suitable for numerous applications, such as serving as an electrode material in lithium-ion systems that employ carbon-based nanocomposites. Introducing heteroatom dopants into graphite can enhance its surface area, porosity, and electrical conductivity, while also improving the stability and durability of the electrode materials, thereby yielding more efficient and longer-lasting lithium half-cells. Nonetheless, the resulting properties depend strongly on the specific dopant used. Challenges such as sluggish solid-state diffusion during rapid charging and unstable SEI layers under high current densities necessitate tailored structural designs to address these issues [23]. Consequently, engineered graphite nanocomposites can be broadly divided into the following categories, enabling the design of materials with optimized ion/electron transport pathways, interfacial chemistry, and structural stability: (i) graphite/carbon composites, (ii) graphite/silicon systems, (iii) graphite/metal oxide composites, and (iv) surface-engineered graphite.

2.2.1. Graphite/carbon nanocomposites

Recent studies indicate that hybridizing graphite with other carbonaceous materials—such as biochar, disordered carbon, graphene, and/or carbon nanotubes—offers a promising route to improve rate performance and control SEI formation. Incorporating biomass-derived carbon introduces hierarchical porosity and numerous new surface sites, which can promote the development of inorganic-rich, mechanically stable SEI layers by enlarging the electrode–electrolyte interface, mitigating local current density, and shortening Li^+ diffusion paths. However, an excessively large surface area can cause irreversible capacity loss due to enhanced electrolyte decomposition. Therefore, an optimal compromise between pore architecture and degree of graphitisation is essential, for example through conductive carbon networks based on graphene and CNT frameworks, to ensure efficient electronic percolation, particularly under high C-rate operating conditions [24].

Mechanistically, these composites provide a more balanced response in galvanostatic intermittent titration measurements, owing to enhanced electrochemical kinetics achieved by reducing the charge transfer resistance (Rct) and increasing the apparent Li^+ diffusion coefficients (D_Li^+), as typically determined by electrochemical impedance spectroscopy (EIS). **Rocky et al**. (2025) reported that a graphite composite incorporating phosphorus-functionalized carbon delivered an initial discharge capacity of 1486 mAh g−1 and a reversible capacity of

530 mAh g−1 at a current density of 100 mA g−1 after 100 cycles, outperforming conventional graphite [25]. Similarly, **Wuet al.** (2024) showed that carbon fibers improved ion storage due to additional active sites arising from a multifunctional core–shell architecture in which carbon fibers are reinforced with a carbon matrix [26]. Furthermore, their work demonstrated that although carbon fibers are prone to rapid capacity fading during lithiation because of volume expansion, engineering the morphology with an appropriate carbon matrix enhances the mechanical robustness of the composite for Li^+ storage. Collectively, these findings highlight that advanced composite designs are crucial for realizing efficient, sustainable energy technologies and high-performance structural batteries.

2.2.2. Graphite/silicon nanocomposites

The technological advantages of silicon are central to designing sustainable electrode materials; however, its high theoretical capacity of ~4200 mAh g^{-1}, while superior among alloy-type anode materials, deteriorates during lithiation because a ~300% volume expansion causes particle pulverization and destabilizes SEI formation. To address this, nanostructured silicon domains embedded within graphitic matrices mitigate the volume change by accommodating stress build-up and maintaining electrode integrity. Consequently, interfacial engineering strategies such as gradient architectures or carbon coatings can regulate continuous SEI growth. These structural designs provide a stable host for silicon nanoparticles, with graphite serving as a mechanical buffer through a conductive framework. Key trade-offs in such composites include challenges in scalable manufacturing, complex synthesis routes, and lowered initial coulombic efficiency. Nonetheless, for large-scale applications, graphite/Si composites hold strong potential to enhance energy density while preserving acceptable cycling stability [27–29].

Haluska et al. (2023) demonstrated the environmental sustainability of lithium-ion batteries by producing carbon-rich nanoscale silicon carbide from barley husks (nSiC/C), which can be graphitized at atmospheric pressure at 2400 °C, [30]. Their composite delivered a capacity of 294 mAh g^{-1} and showed enhanced capacity retention at high current densities (1 and 2 C) compared with commercial graphite, maintaining 80% of its specific capacity over 175 cycles at 1 C. **Maddippatla et al.** (2026) investigated several anode nanocomposites used as anode materials, designated carbon@silicon (C@Si) and graphite@carbon@silicon (G@C@Si) [31]. Their physicochemical characterization confirmed a core–shell configuration, as seen in surface morphologies by SEM and internal structures by TEM. The structure–performance relationship revealed that the G@C@Si nanocomposite offered superior electrochemical performance relative to the other nanocomposites. Nanosilicon was incorporated into the graphite framework via mechanical milling, and XPS elemental analysis verified the core–shell architecture, consistent with the microscopy data. This correlation between pore structure and electrochemical behavior yielded an initial discharge capacity of 1724 mAh g^{-1} and a high initial Coulombic efficiency of 87.37%.

Han et al. (2019) reported that their fabricated electrode material, consisting of an interlinked network of graphene sheets encapsulating silicon, delivered outstanding cycling stability, maintaining a high capacity of 1616.1 mAh g^{-1} after 100 cycles at a current density of 1 A g^{-1} [32]. This performance was attributed to the dual protective role of the interconnected network structure, which enhanced electrical conductivity while accommodating volume expansion and mitigating sluggish ion transport. **Li et al.**, 2023, they reported the structural characteristics of N-doped, porous, flexible vertical graphene sheets (VGSs), referred to as Si-C/VGSs/graphite [33]. Their work clearly demonstrated that this composite enables directional, channel-guided transport of Li ions. This behaviour arises from the numerous exposed active sites—such as the increased number of accessible edge sites that enhance electrical contact within the composite—along with its flexibility and integrated pore architecture, all of which contribute to improved ion storage and reduced volume expansion of silicon.

2.2.3. Graphite/metal oxide nanocomposites

The increasing deployment of electric vehicles and advanced portable electronics has renewed interest in LIBs that deliver high energy density and long operational lifetimes. In this context, transition metal oxides, particularly tin oxide and iron oxide, have attracted significant attention due to their high theoretical capacities via conversion or alloying reactions. By incorporating nanoscale oxide phases into graphite matrices, it is possible to mitigate interfacial degradation and capacity fading typically observed in conventional graphite, especially under high voltage operation and extended cycling. Such composite designs not only promote synergistic interfacial charge transfer but also boost pseudocapacitive contributions, thereby enhancing the reversible capacity. The improved electrochemical performance justifies integrating metal oxides into graphite frameworks; however, conversion-type reactions are often accompanied by pronounced voltage hysteresis and structural instability. The graphite matrix helps address these drawbacks by providing stress-buffering capability and continuous conductive pathways. Consequently, the resulting composite anode is more reliable, capitalizing on interfacial heterojunction effects that lower the activation energy for Li^+ transport [34–37].

Wang et al. (2025) reported a simple two-step synthesis route for Bi/FeS-G anode materials [34]. The introduction of structural disorder and new surface terminations on Bi/FeS-G led to outstanding electrochemical performance, thereby promoting this research approach for the development of lithium and sodium ion batteries. Through ball milling, they coated graphite with bismuth and iron sulfide to investigate their synergistic structural interactions with graphite nanosheets for Li and Na storage. The resulting material exhibited a reversible capacity of 664.1 mAh g−1 at 1.0 A g−1 for more than 400 cycles, and capacities of 409.4 mAh g−1 at 0.5 A g−1 for over 200 cycles in Li and Na tests, respectively. In a related study, Hsiu-**Fen Lin et al.** (2026), motivated by the rapid expansion of EV usage, examined graphite coated with Nb2O5, ZnO, and NiO to improve lithium anode performance, finding that Nb2O5-functionalized graphite outperformed the other electrode materials [35]. This material demonstrated superior electrode kinetics, characterized by rapid Li^+ transport and diminished charge transfer resistance. **Itahara et al.** (2025) investigated Li storage behaviour by coating graphite with tin to obtain a Sn/G composite and a negative graphite electrode derived from spent lithium-ion batteries [36]. The newly fabricated electrode delivered a capacity of 392 mAh g^{-1} at 0.1 C within a voltage window of 0.005–1.5 V vs. Li/Li^+, demonstrating superior electrochemical performance compared with the negative graphite electrode obtained from waste LIBs. In a related study, **Zhang et al.** (2025) carried out a comparative analysis using conventional graphite coated with a bimetallic sulfide via a one-step solid-state pot reaction [37]. Their nanocomposite—conventional graphite integrated with SnS and MnS, where Li intercalation occurs and the bimetallic sulfides are anchored on exfoliated graphite layers—exhibited a high reversible capacity of 802 mAh g^{-1} after 200 cycles at 0.1 A g^{-1}, an initial coulombic efficiency of 86.43 % at 1 A g^{-1}, and a capacity retention of 83.40 % after 500 cycles. For large-scale applications, this approach appears promising because of the simple one-step solid-state synthesis followed by ball milling with 15 % graphite. Furthermore, their DFT calculations indicated that the presence of the graphite matrix enhances Li-ion transport kinetics.

2.2.4. Interface engineering and artificial SEI design

Nanomaterials possess novel characteristics and possibilities that differ markedly from those of their bulk counterparts. Moreover, these distinctive properties are closely linked to parameters such as particle size, morphology, and size distribution, making these features critical and necessitating their precise and efficient measurement. Consequently, the deliberate chemical engineering of interfacial chemistry, beyond conventional bulk composite fabrication, represents a promising

strategy to enhance the electrochemical performance of graphite. In this context, comprehensive understanding of artificial SEI coatings, heteroatom doping, and surface functionalization not only offers new opportunities but also governs mechanical stability, ionic transport, and the overall SEI composition, for example, determining LiF-rich versus organic-rich layers. State-of-the-art characterization tools, including in situ transmission electron microscopy (TEM), cryogenic TEM, and XPS depth profiling, have demonstrated that robust, inorganic-rich SEI films markedly improve fast-charging durability. Therefore, the development of future graphite nanocomposites should emphasize optimization of interfacial chemistry in tandem with structural design [38–42].

As a protective layer, the primary role of the SEI is to suppress unwanted parasitic reactions, including solvent co-intercalation into graphite and its subsequent reduction, which can cause irreversible capacity loss and graphite exfoliation. The solvent selected for Li-ion electrolytes dictates the SEI composition; therefore, an optimal SEI should result from a well-matched combination of solvent, salt, and additives, providing synergistically high lithium-ion conductivity, effective electronic insulation, and stable SEI formation on the anode. This, in turn, minimizes further electrolyte–electrode decomposition while enhancing mass transport. In addition, the solvent system for graphite anodes should yield a mechanically robust SEI with low interfacial resistance to accommodate volume changes during charge/discharge and to impede dendrite growth. Consequently, empirical SEI evaluation should be coupled with mechanistic insight to assess multiscale regulation strategies, including detailed interphase characterization supported by electrochemical measurements such as coulombic efficiency and Li plating behaviour [38].

In Fig. 2d, high-resolution transmission electron microscopy (HRTEM) reveals crystalline LiF and Li2O domains embedded within an amorphous matrix, giving rise to a mosaic-like architecture with nanoscale phase separation. The presence of the 002 planes of LiF and Li_2O indicates that the SEI is enriched in inorganic components, while the surrounding amorphous regions are predominantly organic, evidencing heterogeneity and nanostructured mixing. The observed lattice fringes are largely associated with these 002 planes, and prior reports have shown that such a composite configuration is mechanically robust, with enhanced cycling performance and interfacial stability. The additive fluoroethylene carbonate contributes to the formation of a stable SEI and suppresses dendrite growth by increasing interfacial energy, whereas Li_2O facilitates rapid Li-ion transport along decomposition pathways. However, polydispersity and structural heterogeneity can also lead to uncontrolled lithium deposition and localized concentration gradients, generating stress and ultimately compromising long-term stability [39,40].

The morphological and elemental distributions after stripping, shown in Fig. 2e, indicate a pronounced change in the lithium metal and its SEI, which now exhibits a tunable pore structure along with a fibrous and partially collapsed framework. This structural evolution reflects the loss of electrochemically active lithium and the formation of electrically isolated “dead” lithium trapped within the SEI matrix. Selected area electron diffraction (SAED) patterns confirm the presence of crystalline Li_2O phases, while elemental mapping shows an approximately uniform distribution of Li, O, F, and C across the remaining structure, implying the coexistence of inorganic (LiF, Li_2O) and organic components. Although Li^+ is strongly solvated in carbonate-based electrolytes, the inorganic species in the SEI possess poor interfacial stability during repeated lithium stripping/plating cycles, which leads to low lithium reversibility, diminished capacity, and reduced coulombic efficiency. Overall, these observations align with previous reports describing the SEI as dynamically unstable and a key contributor to failure mechanisms in lithium metal batteries [39,40].

2.2.4.1. Framing in the context of renewable energy systems. The shift toward renewable energy sources, such as solar and wind, has increasingly drawn attention over the years, particularly regarding the need for sustainable, long-term energy storage technologies. Lithium-ion batteries currently dominate the market and are viewed as a leading candidate for both grid-scale storage to balance supply and demand and for decentralized energy storage. However, their large-scale deployment is limited by performance characteristics that strongly depend on the solid–electrolyte interphase (SEI). From a thermodynamic standpoint, SEI formation is controlled by soluble and decomposable electrolyte products generated at specific electrode potentials, resulting in complex interphases that present both stability and functionality challenges. Recent research highlights that the salt largely dictates the decomposition pathways, the solvent shapes the solvation structure, and the additives enable interphase engineering. These components are typically reduced at characteristic potentials, thereby determining SEI chemistry and interfacial stability, which in turn are crucial for achieving durable, long-cycle operation under fluctuating renewable energy inputs [39–42].

2.2.4.2. Mechanisms and materials insights. For understanding SEI nucleation and stabilization, researchers must look beyond simple ionic conductivity and thermodynamic considerations, particularly considering the extensive literature on heterogeneous surfaces and interfacial engineering. Surface modification can generate defects, vacancies, adsorption sites, and grain boundaries—as illustrated in Fig. 2d—that enable localized electrolyte interactions and thereby enhance performance. Interphases engineered with heterostructure designs have been shown to improve local electron transfer and ion concentration, while promoting a uniform SEI with high mechanical robustness. These benefits largely arise from artificial coatings applied to graphite surfaces and composite electrodes. Electrolyte additives such as fluoroethylene carbonate (FEC) and vinylene carbonate (VC) undergo preferential decomposition, effectively producing an SEI that is rich in inorganic components. This promotes the formation of stable SEI layers, directly improving interfacial stability and electrochemical performance, and ultimately supporting long-term cycling and renewable energy applications [38–42].

2.2.4.3. Advanced techniques and future direction. Recent investigations have progressed from purely empirical testing to advanced characterization and modelling, enabling more detailed analysis of SEI formation mechanisms. Operando TEM and cryo-TEM, as illustrated in Fig. 2d, allow direct visualization of interphase evolution under realistic operating conditions, thereby revealing critical information on dynamic morphological and structural transformations. Additional widely used, complementary techniques include X-ray photoelectron spectroscopy (XPS), which is highly effective for depth-resolved analysis of compositional gradients arising from electrolyte decomposition across SEI layers, and density functional theory (DFT) calculations, which offer atomistic-level insights into lithium adsorption and reaction kinetics at electrode interfaces. Combining these experimental and computational approaches shifts the focus from electrolyte design toward deliberate interphase engineering, a transition that is vital for constructing predictive models and rational design strategies to advance next-generation energy storage technologies and to realize robust, sustainable energy storage systems [38–42].

The ability of graphite to enhance the high-rate charge performance and discharge activity of lithium ions mobility during intercalation and deintercalation within the graphite structure is of paramount importance. This proves that the graphite anode has a higher ability to increase the electrocatalytic activity of Li^+ transport spans microscopic to macroscopic scales and is influenced by the microstructure, texture, and powder properties of. The utilization of graphite as an electrode has gained popularity in the battery industry, to increase or improve the performance of batteries as it is also dependent on the electrodes where the solid electrolyte interphase (SEI) facilitates the movement of lithium

ions in a solvated state to reach the surface of the graphite. For an efficient intercalation into graphite layers, lithium ions first undergo reduction and eventually through the diffusion pathways, are driven by gradient concentrations and electric fields. The structural property of graphite like microstructures, SEI membrane composition synergistically affects the rate of lithium-ion diffusion where thin SEI membranes, larger interlayer spacing and small layer diameters facilitates the fast ion transportation. Thus, doping with hetero atoms into the graphite surface and layers, tailor the structural and morphological properties and promotes the transport rate capabilities of lithium ions into graphite, thus increased performance as observed Fig. 2a-c [43].

The material composition, particle size and shape as well as the textural properties of graphite can be seen that lithium-ion mobility is affected by these properties, the relationship of lithium ions transport mechanism and physiochemical properties is schematically illustrated in Fig. 3 [43]. The study finds that an isotropic arrangement and spherical particles enhance the diffusion of ions by providing better pathways. However, larger particle sizes increase the ion diffusion path, while smaller particles increase diffusion rates but reduce packing density, ultimately affecting overall battery capacity. The study suggests granulating small particles into larger ones to balance the packing density and ion diffusion rates. It concludes that challenges related to the microstructure and properties of graphite particles require tailored solutions to improve the charge - discharge performance of lithium-ion batteries [43].

In lithium-ion batteries (LIBs), electrolytes typically consist of low-molecular-weight organic solvents mixed with an aprotic salt solution. At the graphite anode, these electrolytes undergo decomposition, resulting in the formation of the solid electrolyte interphase (SEI) layer. This layer plays a crucial role in determining both the immediate efficiency and long-term capacity retention of the cell. In Fig. 3d the energy diagram it can be observed that electrolyte degradation and capacity deterioration can be salvaged using these methods to achieve a durable cell performance. The differences in anode, cathode and electrolyte energy levels with emphasis on stability window defined by the electrolyte, and the energy gap of the highest and lowest molecular orbitals, highest occupied molecular orbital (HOMO) and lowest unoccupied molecular orbital (LUMO). Boosting the energy density requires maximising the energy difference between the anode and cathode. However, the intercalation potential of the graphite electrode falls below the electrolyte's reduction potential of the electrolyte, which triggers electrolyte decomposition and subsequent SEI formation at the graphite surface during the charging process, as seen in Fig. 3d [44].

The storage mechanism in lithium-ion batteries is following the concept of "rocking chair "concept. The Li ion transport is driven by the concentration difference between the cathode and anode, enabling intercalation and deintercalation into and out of the electrode materials during the charging and discharging process. As shown in Fig. 4a, a typical $LiCoO_2$/C architecture demonstrates this process. During the charging process, the Li ions are extracted from the cathode material and, under the influence of an external electric field, migrate through the electrolyte and separator to be intercalated into the graphite anode During discharge, the Li + ions are deintercalated from the anode and reinserted into the cathode, completing the reversible process and thereby contributing to the reversible capacity of the battery. The charge and discharge reaction equation are as follows [45]:

$$\textbf{Cathode reaction}: \boldsymbol{LiCoO_2 \leftrightarrow Li_{1-x}CoO_2 + xe^-} \quad (5)$$

$$\textbf{Anode reaction}: \boldsymbol{6C + xLi^+ + xe^- \leftrightarrow Li_xC_6} \quad (6)$$

$$\text{Total reaction}: \boldsymbol{LiCoO_2 + 6C \leftrightarrow Li_{1-x}CoO_2 + Li_xC_6} \quad (7)$$

This research involved the assembly of a coin cell using an anode composed of artificial graphite (AG) paired with an LFP cathode [45]. The specific capacity of the LFP cathode allowed tuning the specific capacities of the graphite anode by adjusting its mass. This configuration allowed for the investigation of the cycle performance of the graphite electrode, its operational principles, and the overall storage mechanism of the battery. In LIBs, an anode with a specific capacity below 340 $mAhg^{-1}$ is referred to as a pure intercalation anode in lithium-ion batteries (LIBs). In such a system, only the mechanism of intercalation and de-intercalation of Li ions within the graphite structure control the process of charging and discharging. Anodes with specific capacities above 340 $mAhg^{-1}$ involve both Li-ion intercalation and Li-metal deposition processes, thus classified as Li-ion/Li-metal composite anodes (see Table 1). The capacity contributions of each mechanism can be estimated based on the theoretical specific capacities: 340 mAhg−1 for Li-ion intercalation and 3860 mAhg−1 for lithium-metal deposition. The anode capacities of 340, 450, 600, and 3860 $mAhg^{-1}$, are represented as LiC_6, $Li_{1.36}C_6$, $Li_{1.91}C_6$, and Li, which correspond to the mechanisms of pure intercalation, hybrid intercalation-conversion, and conversion, respectively, Fig. 3b, c [45].

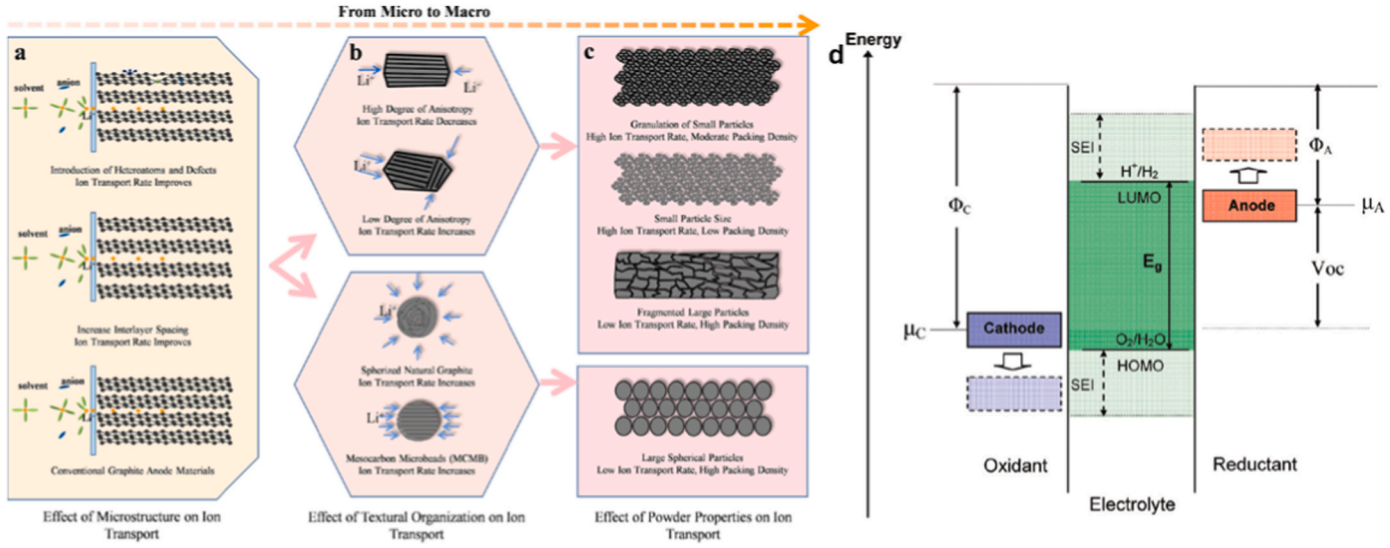

Fig. 3. (**a-c**) The particle size effects on Li^+ transport. Reproduced with permission from Ref. [43], © 2025 Elsevier Ltd. (**d**) Open-circuit energy diagram of an aqueous electrolyte; work functions of anode (ΦA) and cathode (ΦC); the window of the electrolyte' thermodynamic stability (Eg). the formation of an SEI layer requires a kinetic stability (μA > LUMO and/or μC < HOMO). Reproduced with permission from Ref. [44], Copyright © 2010 American Chemical Society.

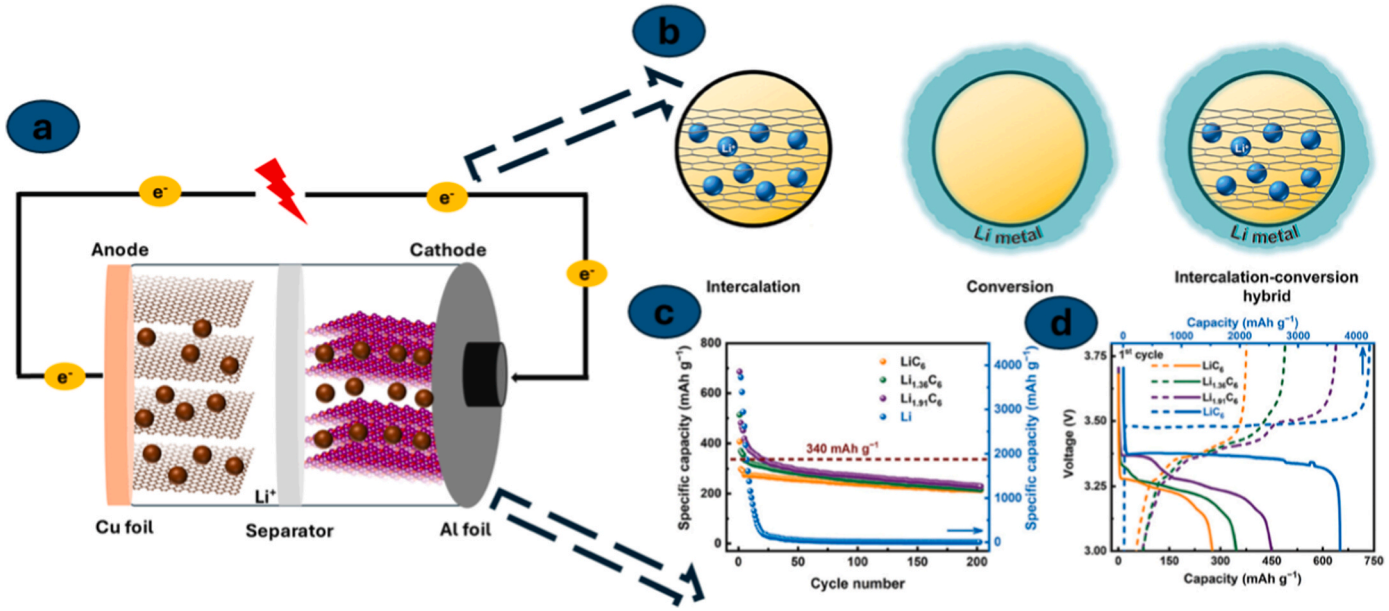

Fig. 4. (**a**) Schematic representation working principle of LIBs, (**b**)The Li^+ storage in graphite [45] (**c**) Discharge capacity of full cells [45]; (**d**) the capacity-voltage curves [45]. Reproduced with permission from Ref. [45], © 2024 Wiley-VCH GmbH.

Table 1
The capacities of the anode and the corresponding molar ratios are related to different lithium storage mechanisms [45].

Li storage mechanism	Capacity (mAh g^{-1})	Capacity ratio between conversion and Intercalation	Stoichiometric ratio
Intercalation	340	0	LiC_6
Intercalation-conversion (hybrid)	450	0.36	$Li_{1.36}C_6$(0.36Li + LiC_6)
	600	0.91	Li $_{1.91}$ C_6 (0.91 Li + LiC_6)
Conversion	3860	-	Li

The research investigated the electrochemical properties of a cell comprising an LFP cathode and graphite anodes configured at various lithium storage levels (LiC_6, Li $_{1.36}$ C_6, Li $_{1.91}$ C_6) Table 1 [45]. Each anode experienced a similar decrease in discharge capacity, with the most obvious reduction occurring during the initial cycles. This was contributed to the formation of the SEI layer, which consumes active lithium and diminishes capacity. The SEI layer struggled to accommodate volume variations, resulting in its frequent cracking and reformation, which further deplete active materials. A stable SEI is formed when the capacity falls below 340 $mAhg^{-1}$, allowing for a more consistent cycling performance. However, different anode storage behaviours in anode require different SEI compositions, presenting a significant challenge in the design of a stable SEI for composite anodes [45].

Carbon nanoparticles (CNPs) have received extensive studies since their discovery about a decade ago. This review provides an in-depth evaluation of current graphite nanocomposites, highlighting their dual functions in maintaining structural integrity and storing electrochemical energy. The discussion begins with an overview of the technological background, the motivation behind the development of graphite anode materials, and the integration of Li^+ ion storage within graphite hosts. A systematic classification of design structures-such as Biochar, and graphite is then presented. Strategies aimed at improving ionic conduction, electronic transport, and capacity efficiency are examined in detail. Electrochemical performance metrics such as capacity, energy density, and cycling stability are reviewed using data from the recent literature. The review concludes by highting the potential application of graphite nanocomposites in lithium-ion batteries that demand high capacity and energy density, and it outlines future research directions to boost performance, scalability, and real-world applicability [46].

In top-down methods, nanoparticles are formed by breaking down larger pieces of precursor materials into desired nanomaterials. This includes arc-discharge, laser ablation, chemical, and electrochemical techniques. In contract, bottom-up approaches involve molecular assembly of precursors through processes such as combustion, microwave-assisted methods, and hydrothermal methods. These methods have successfully produced carbonaceous additives, such as carbon nanotubes, reduced graphene oxide, and pyrolyzed carbon derived from precursors such as pitch, sugars, and heteroatom polymers; these carbonaceous additives play an important role in the construction of hierarchical structures of micrometre-sized within graphite/carbon composites. They also contribute to tailoring the morphology and surface properties, resulting in the composites with good structural stability, strong adhesion, high electrical conductivity, high tap density, and optimized interface chemistry-ultimately achieving both high capacity and long cycling stability [47,48].

2.3. *Graphite/biochar*

Biochar-based lithium anode materials derived from biomass show significant promise; however, their naturally low conductivity and increased porosity, along with shortened diffusion paths, can be mitigated by incorporating graphite intercalating layers. These layers provide a high surface area and excellent intercalation characteristics, enhancing ion transport capabilities. Studies have revealed that a 3D interconnected pore network modified with iron nanoparticles boosts the specific surface area to 475 m^2/g and improves thermal stability, making it suitable for LIB anode electrodes. The integration of metal nanoparticles into these channels, together with the expanded surface area, enhances lithium-ion storage, enabling the electrode material to achieve a discharge capacity of 1307 mAhg-1 at a current density of 0.1 A/g, with robust cyclic performance that retains 60% after 150 cycles. Due to its abundance and cost-efficiency, this method is considered an attractive candidate for the graphite nanocomposite electrode material in next-generation electrochemical devices. The chemical processes and reactor setup crucially influence the physicochemical properties of biochar, with production techniques being critical. Typically produced by pyrolysis, biochar results from the decomposition of biomass at

200–1300 °C under low oxygen conditions or in inert gases (refer to Fig. 5). Pyrolysis is classified based on the heating rate and duration, into slow, fast, flash, and intermediate methods [49,50].

2.3.1. Biochar production methods

Using biochar as an energy material, the source is derived from diverse sources such as agricultural by-products and solid waste, and it emerges as a promising renewable and sustainable energy material with significant potential as a low-cost, carbon-rich precursor for electrode materials in lithium-ion batteries. In this review, we first introduce background of biochar, including process techniques from agricultural waste, treatment methods, etc. the characteristics of biochar are influenced by the type of feedstock and the conditions under which pyrolysis is performed. The employment of crop waste, including straws and husks, can promote both renewable energy initiatives and sustainable resource management. Proper handling and disposal of agricultural waste is essential to prevent wasting resources and minimise potential hazards. Biochar (BC) is produced from biomass through thermochemical processes such as torrefaction, pyrolysis, and gasification, each distinguished by different operating temperatures. Torrefaction, which occurs at 200–350 °C, results in partial carbonization with up to 50 wt% carbon content, which can be increased to 80 wt% using additional methods, though it often lacks the necessary conductivity for anodic material applications. Conducted at above 400 °C in the absence of oxygen, pyrolysis enables a more comprehensive breakdown of biomass components like lignin, cellulose, and hemicellulose, producing BC and bio-oils [51–53].

Pyrolysis employs various heating methods and apparatus, influencing the quality and number of products generated. In contrast, gasification uses an oxidant and operates at temperatures exceeding 800 °C to generate a gas mixture containing components such as carbon monoxide and hydrogen. While pyrolysis produces carbon-rich byproducts, gasification produces substances with a high ash content and reduced carbon levels, making them impractical for battery applications [54].

2.3.2. Pretreatment methods

Thermochemical pretreatment stands out among the diverse methods that aim to optimize fermentation in biofuel production. By employing a combination of heat and chemical compounds, this technique converts biomass such as sugarcane bagasse in employing bioil, or biogas. It is noted to be more versatile and effective compared to other pretreatment approaches, particularly excelling in areas such as reduced chemical use, lignin breakdown, and potential for large-scale application [55].

2.3.3. Chemical activation

Chemical treatments, including the use of acids and bases, improve the yield and quality of biochar by altering the properties of biomass. Perchloric acid is particularly effective because of its high acidity and stability, which improves the features of biochar, although it is extremely corrosive. These treatments decrease carbon content, reduce tar formation, release volatile compounds, and expand the pore structure. For example, KOH chemically activates biochar, enhancing its porosity and surface area. Chemical activation is more effective than physical activation, yielding biochar with greater surface areas and porosity at lower temperatures. This is followed by high-temperature pyrolysis for further enhancement [56,57].

2.3.4. Thermal activation

The thermal breakdown of waste biomass through pyrolysis serves as an economical approach to fabricate electrodes for microbial fuel cells, emphasizing its advantages of substantial surface area and high porosity. Pyrolysis, conducted without oxygen, transforms biomass into biochar, syngas, and bio-oil through chemical processes. It is classified into fast and slow pyrolysis; fast pyrolysis involves quick heating, yielding a variety of products, whereas slow pyrolysis heats the material gradually, producing biochar that enhances soil by modifying the biomass structure. The production of biochar through slow pyrolysis is effective, with favourable outcomes and with gas by-products beneficial for cogeneration. The efficiency of the process is affected by the temperature of pyrolysis: at lower temperatures, it produces fewer phenolic, carbonyl, and alkyl groups; between 400 and 500 °C, it reduces phenolic -OH and increases quinoid C=O; above 500 °C, the process can improve aromaticity and conductivity without altering oxygen-functional groups. Higher temperatures improve the biochar's surface area and porosity due to organic material breakdown and micropore development. These modifications alter biochar's electrochemical characteristics, affecting microbial activities and exposing the lignin core. Biochar derived from sugarcane bagasse reveals increased carbon content as temperatures rise, with notable retention of lignin and degradation of hemicellulose and cellulose [58,59].

2.3.5. Graphite/biochar applications

Graphite nanocomposites in lithium technology face several hurdles, such as elevated expenses, inefficient energy use, and sustainability concerns stemming from electrode deterioration. Although the influence of acid alterations on biochar's surface and battery efficiency remains largely unclear. The use of carbon sourced from biomass presents a sustainable method for advancing battery technology. The paper also examines the shortcomings of graphene sheets in lithium-ion batteries, particularly due to suboptimal Li^+ intercalation kinetics in graphite anodes. Implementing surface treatments and incorporating heteroatoms or carbon-based additives are proposed to counteract undesired side reactions. Biochar derived from biomass waste helps create a stable and advantageous solid electrolyte interface (SEI) on graphite particles, leading to a thin, consistent SEI. This improves rate performance by supporting consistent and rapid reaction kinetics and effective lithium-ion conduction [60–62].

Its mesoporous architecture mitigates particle aggregation and encourages a uniform distribution of metal particles, boosting catalytic efficiency. Biochar can trap metal ions within its pores, minimizing the

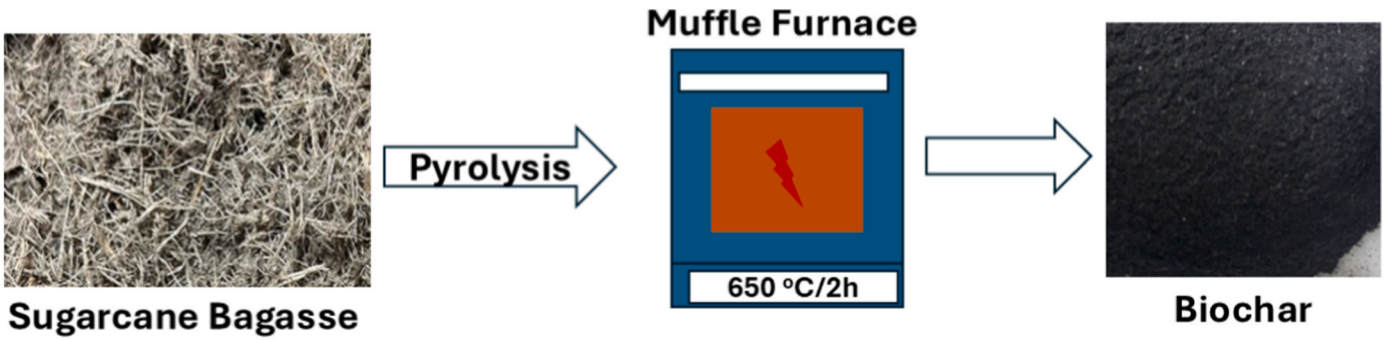

Fig. 5. Schematic illustration of transforming sugarcane bagasse into biochar via a muffle furnace for pyrolysis.

leaching of metals. The function of biochar nanocomposites is influenced by both the type of biomass used and the conditions under which they are prepared. Thanks to their conductive and porous features, they are ideal for electrode applications, though their effectiveness can be affected by inorganic content, the nature of the matrix, and surface functionalities. The properties and applications of biochar, especially its high porosity and nitrogen-inclusive functional groups, make it an excellent material for supercapacitor electrodes. With 45-60% carbon and minimal inorganic content, biochar provides increased chemical diversity through heteroatoms, unlike carbon black. It serves as a catalyst or catalyst support in biofuel production due to its surface functional groups, which facilitate functionalization and metal precursor support. Although biochar's aromatic crystalline structure enhances its porosity and surface area for carbon capture, its limited porosity, surface area, and polar surface groups can constrain its application in specific technologies like fuel cells and photoactive materials [63–65].

Chen *et al*, 2021 demonstrated the use of biochar derived from *Eichhornia crassipes* which is regarded as a deadly floating plant [66]. Their study showed that conversion of biomass into valuable biochar material for lithium-ion technology offers new opportunities for both environmental pollution mitigation and energy efficiency for energy storage technologies like lithium technology. The textural properties of the biochar material exhibited a specific surface area of 278.56 m^2 g^{-1} induced by the introduction of heteroatoms (3.42% N, 20.82% O, and 0.83% S) during chemical activation with KOH, with a highly recorded initial reversible specific capacity of 697 mAh·g^{-1} at a current density of 50 mA g^{-1}. The interconnected honeycomb porous structure is attributed to the enhanced electrochemical properties, with fast Li^+ transfer, electrolyte infiltration and presence of heteroatoms. **Yan *et al*, 2019**, developed biochar anode material derived from wheat straw with the same chemical activation using KOH. And the recorded discharge capacity was 310 $mAhg^{-1}$ after 100 cycles at 0.1 C rate [67].

The elemental makeup of biochar and its reliance on the original materials and the conditions under which it is produced. Biochar is recognized as an advantageous support for catalysts because it helps reduce leaching and improves recycling processes. Successful catalysts typically have a high surface area, excellent porosity, environmental robustness, and electron conductivity. Nevertheless, carbon supports face issues such as corrosion, which results in detachment and clumping, which weakens bonding. In lithium-ion batteries, these carbon supports can become unstable, experiencing corrosion of the cathodic electrode at high potentials, which deactivates surface sites and decreases performance due to de-intercalation of Li ions [66,67].

The impact of corrosion on electron transport and reactivity, emphasizing biochar's role in enhancing material properties, particularly in ring-opening reactions. Developing a novel approach to the study of carbon-based materials demonstrates the robust and adaptable nature of carbon-based materials, with an emphasis on the performance of biochar-derived nanocomposites in both acidic and alkaline environments. These nanocomposites are crucial for lithium-ion intercalation, as they depend on a stable solid electrolyte interphase (SEI) for effective ion transport. Additionally, research focusses on the development of economical carbon-based nanomaterials, highlighting the challenge of high costs, influenced by the density of surface functional groups in graphite nanocomposites, Table 2 [68,69].

2.3.6. Graphite nanocomposites in lithium-ion battery

2.4. Energy storage devices

The growing demand for efficient and environmentally friendly energy materials that offer flexibility, a long lifespan, and low cost is on the rise. Although lithium-ion batteries (LIBs) are crucial for portable electronics, they are hampered by the scarcity of lithium, high costs, and safety issues. Thus, sodium-ion batteries (SIBs) are gaining attention as a viable alternative because of their abundance, reduced cost, energy density, and redox potential, which are comparable to those of LIBs. Additionally, other non-lithium batteries, like K-ion, Al-ion, Mg-ion, and Ca-ion batteries, are being explored for future energy storage technologies. There are challenges to optimize electrolytes and electrode materials in battery technology. Although graphite performs well as an anode material for LIBs, it is not effective for SIBs. Consequently, there is a pressing requirement to develop superior electrode materials for non-lithium-ion batteries. Biomass derived carbon has recently been identified as promising candidates due to their outstanding morphological characteristics and high theoretical capacity as host materials for metal-based ion batteries, with notable specific capacities for Li, Na and K [74,75].

Table 2
Artificial graphite synthetic methodology and electrochemical analysis.

Precursor	Method Temperature (oC)	Specific Capacity (mAh)	Cycle life	ICE	Ref
CO_2-derived carbon	Graphitisation @ 2800	297–378.1	~100% after 300 cycles	72.6–80.5	[70]
Anthracite	Graphitisation @2700 using boron oxide catalyst	337.2	500 cycles at 2 C	89.2	[71]
Bituminous coal	Graphitisation @2000-2800	310.3	100	95.3%	[72]
Needle coke	Graphitisation @2700	352.6	50	99.1	[73]

The electrochemical properties of two carbon-based materials, L-HC-2500 and L-AGs, are investigated at a C-rate of 0.1 C within a voltage range of 0.01–2.0 V. The L-HC-2500, composed of disordered carbon, displays sloping voltage profiles without significant plateaus, achieving a reversible capacity of approximately 120 $mAhg^{-1}$ over 100 cycles. This suggests that lignocellulose does not transform into graphite at temperatures as high as 2500 °C in the absence of a Fe catalyst, as shown in Fig. 5c, e. In contrast, L-AGs paired with an Fe catalyst display modified voltage profiles, as shown in Fig. 5b, d. The L-AG-2500 reaches a reversible capacity of about 344 $mAhg^{-1}$, like that of commercial natural graphite (around 350 mAhg-1), and exhibits standard lithium-ion intercalation characteristics. Nevertheless, the initial Coulombic efficiency (ICE) of L-AGs (79%-82.5%) lags that of commercial graphite (90%-94%), suggesting more parasitic reactions like the reductive decomposition of the electrolyte [76,77].

The necessity to enhance Initial Coulombic Efficiency (ICE) via surface treatments and particle property optimization. Electrochemical characteristics were analysed using differential capacity plots, identifying a reduction peak at 0.75 V during the initial discharge stage. This phenomenon, attributed to the breakdown of the electrolyte and the formation of SEI, accounts for the low ICE observed in artificial graphite based on lignin (L-AG), as presented in Fig. 6f. With an increase in graphitisation temperature, this peak shifts to lower voltages, its intensity diminishes, and surface properties change, resulting in diminished interface formation with the electrolyte. Subsequent reduction peaks point to lithium-ion insertion into the graphene layers. In the second cycle, all L-AGs undergo similar reactions and preserve capacity; a stable SEI layer impedes further decomposition, as indicated by the absence of formation-related reactions. Consequently, this leads to stable electrochemical behaviour and enhanced Coulombic efficiency starting from the second cycle [78,79].

The cycling stability and rate capability of the L-AG-2500 anode. It reports that the capacity retention remains at approximately 100% after 100 cycles with a reversible capacity of 347 $mAhg^{-1}$ at a 0.1 C rate. The coulombic efficiency stabilizes at ~99% due to the formation of a stable SEI layer. The voltage profiles indicate consistent electrochemical behaviour throughout the cycles. A comparative analysis highlights the

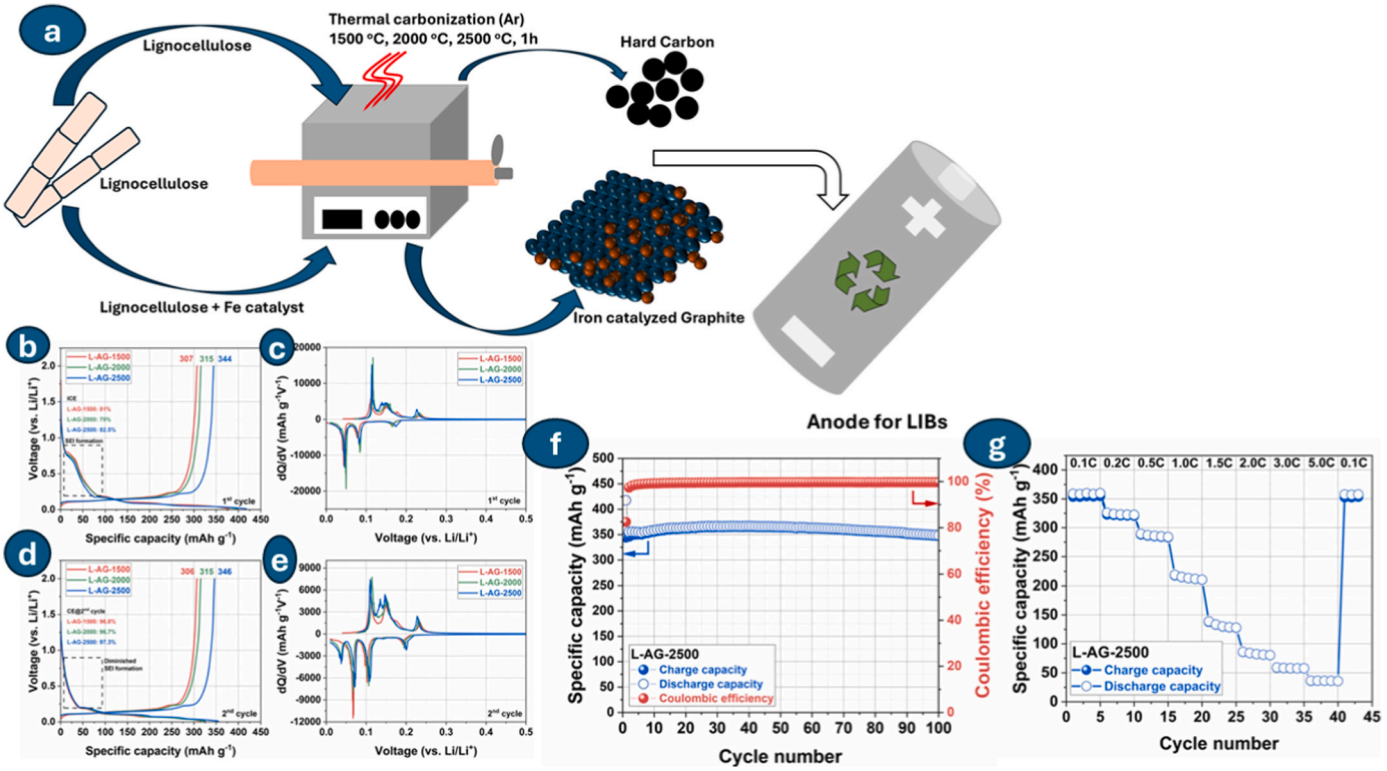

Fig. 6. Electrochemical assessment of anode materials L-AG-1500, L-AG-2000, and L-AG-2500: (**a**) Schematic illustration of hard carbon and iron catalysed graphite, (**b**) Galvanostatic charge-discharge curves and (**c**) associated differential capacity (dQ/dV) plots for the first cycle. (**d**) Galvanostatic charge-discharge curves and (**e**) associated differential capacity (dQ/dV) plots for the second cycle. Cycling stability of L-AG-2500 at a C-rate of 0.1 C is observed along with (**f**) its respective galvanostatic charge and discharge profiles. (**g**) Performance test of L-AG-2500 across varying C-rate conditions from 0.1 C to 5.0 C. [80], © 2025 Elsevier.

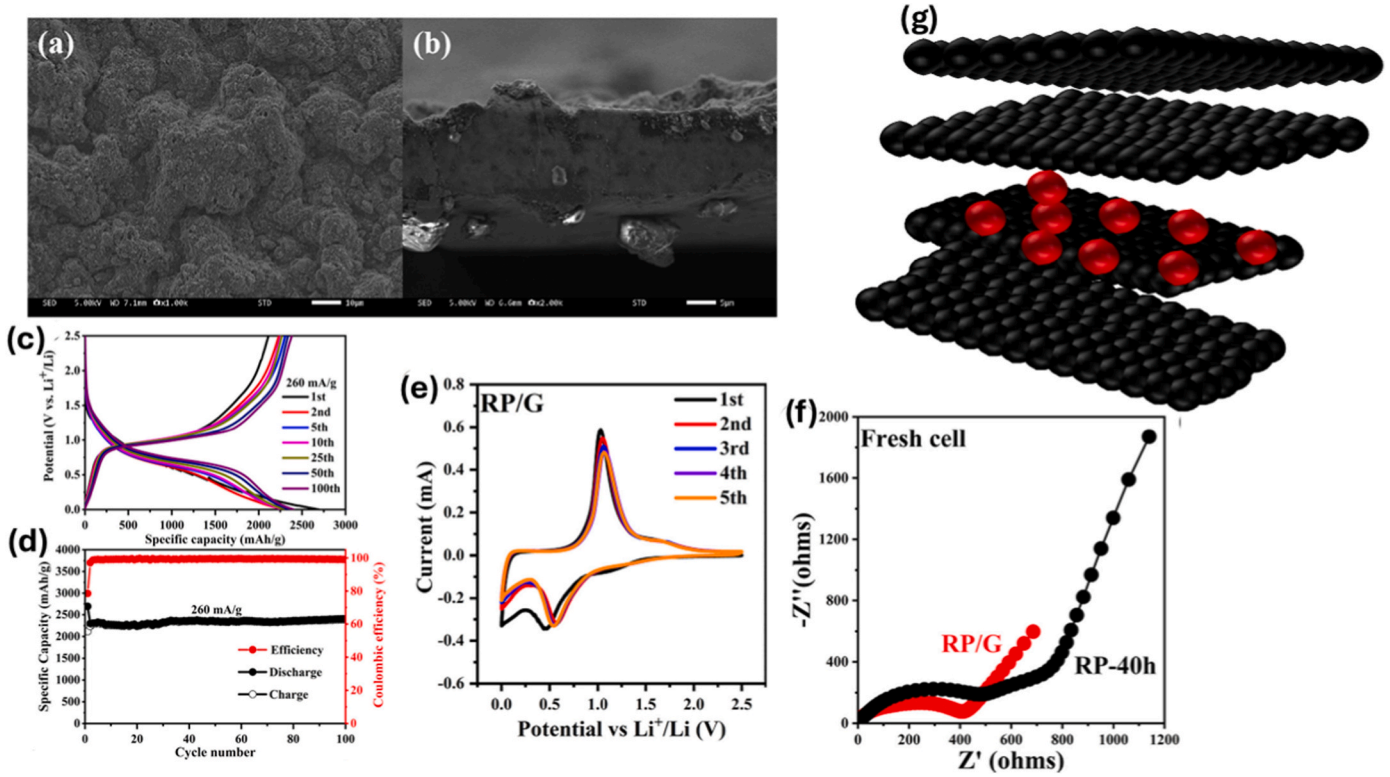

Fig. 7. SEM Images (**a**) Top view (**b**) Cross section (**c**) Charge-discharge curves(**d**) Initial Charge-discharge curve at 260 mAh1(**e**) CV curves (**f**) Nyquist plot. (**g**), Schematic drawing of red phosphorus between graphite layers [82]. (For interpretation of the references to colour in this figure legend, the reader is referred to the Web version of this article.)

superior performance of L-AG-2500 over other lignocellulose materials, with a notable reversible capacity of ~344 $mAhg^{-1}$. The anode's rate capability is tested at various C-rates, showing decreasing reversible capacities from ~344 $mAhg^{-1}$ at 0.1 C to ~35 $mAhg^{-1}$ at 5.0 C, Fig. 6f, g [80,81].

The performance and structural traits of L-AG-2500, a type of graphite anode, are noteworthy. At a rate of 5 C/0.2 C, capacity retention was roughly 10%, and the material showed anisotropic features along a well-developed basal plane. Li^+ ions are expected to intercalate via the edge plane, which implies that an isotropic surface coating could improve L-AG-2500's Li^+ ion diffusion and rate performance. Despite the reduced plateau stages and increased overpotential at elevated C-rates, L-AG-2500 showed notable capacity recovery when the C-rate reverted to 0.1 C, reflecting robust structural stability. These results underscore the need for further research on graphite anodes, especially those from lignocellulose, to improve their rate capability for rapid charging and discharging uses, Fig. 6g [81].

The findings tackle the issue of boosting the capacity and stability of graphite integrated with red phosphorus, utilized as anodes in lithium-ion batteries, attributed to its mechanical endurance. A top-down cross-sectional view in Fig. 7(a, b) confirms the structural integrity, as no cracks are detected. Fig. 7c presents the charge-discharge profiles of the RP/G electrode at a current density of 260 mA/g, where the first discharge and charge specific capacities are recorded at 2691 $mAhg^{-1}$ and 2114 $mAhg^{-1}$, respectively, with an initial Coulombic efficiency of 78.6%. The irreversible capacity is due to the formation of a solid electrolyte interface (SEI) film during the initial cycle. Conductivity is enabled by the delocalized π-electrons within the carbon atoms' sp2 bonds, generating a conductive electron network over the graphene sheet, thus allowing electrons to move freely. The study indicates that RP@G maintains a stable reversible capacity of 2383 $mAhg^{-1}$ over 100 cycles at 260 mA/g, as shown in Fig. 7d, with a capacity retention of 1713 $mAhg^{-1}$ after 600 cycles. The RP/G composite's catalytic strategy indicates the promise of phosphorus and carbon-based materials as anodes for affordable and high-capacity LIBs. The nanocomposite's benefits are tied to its defective and disordered design, which improves lithium-ion accommodation, enhances electronic conductivity, and facilitates lithium-ion diffusion. These attributes offer a broadened interaction surface with lithium ions, efficient electron transport, and minimized strain, ensuring consistent cycling performance by illustrating the electrochemical reaction mechanism [82].

In Fig. 7e, CV curves illustrate the initial cycles at a scan rate of 0.1 mV/s. A broad peak between 1.0 and 1.3 V appears in the first cathodic scan, linked to SEI film formation, and this peak does not appear in later cycles, indicating SEI formation primarily occurs in the initial cycle. The broad peak at 0.46 V in the first cathodic scan results from multistep lithiation reactions, while the dominant cathodic peak at 0.54 V in subsequent scans is attributed to ongoing lithiation. In the anodic scans, the main peak near 1.07 V signifies the reversible delithiation process. CV curves from the 2nd to the 5th cycles align closely, suggesting a stable electrode structure. Contributions of diffusion-controlled intercalation and the capacitance process were quantified, revealing an increase in electron transfer within the first 10 cycles, as depicted in Fig. 7f. These discoveries imply that the RP/G electrode enhances electrical conductivity, accelerates charge-transfer, and maintains stable lithium-ion diffusivity during charge-discharge cycles, ensuring impressive capacity and stability. Thus, the conductivity of graphene arises from its unique electronic band structure, a quantum mechanical property, rather than from typical metallic conduction. Fig. 7g presents a schematic of red phosphorous LIB [82].

The study tested various proportions of precursors to synthesise After fully dispersing, it was stirred and dried at 70 °C and then transferred to a tubular furnace, heated to 600 °C at a rate of 2 °C min^{-1} in the atmosphere of argon, and held for 1 h. Fig. 8a illustrates that biochar

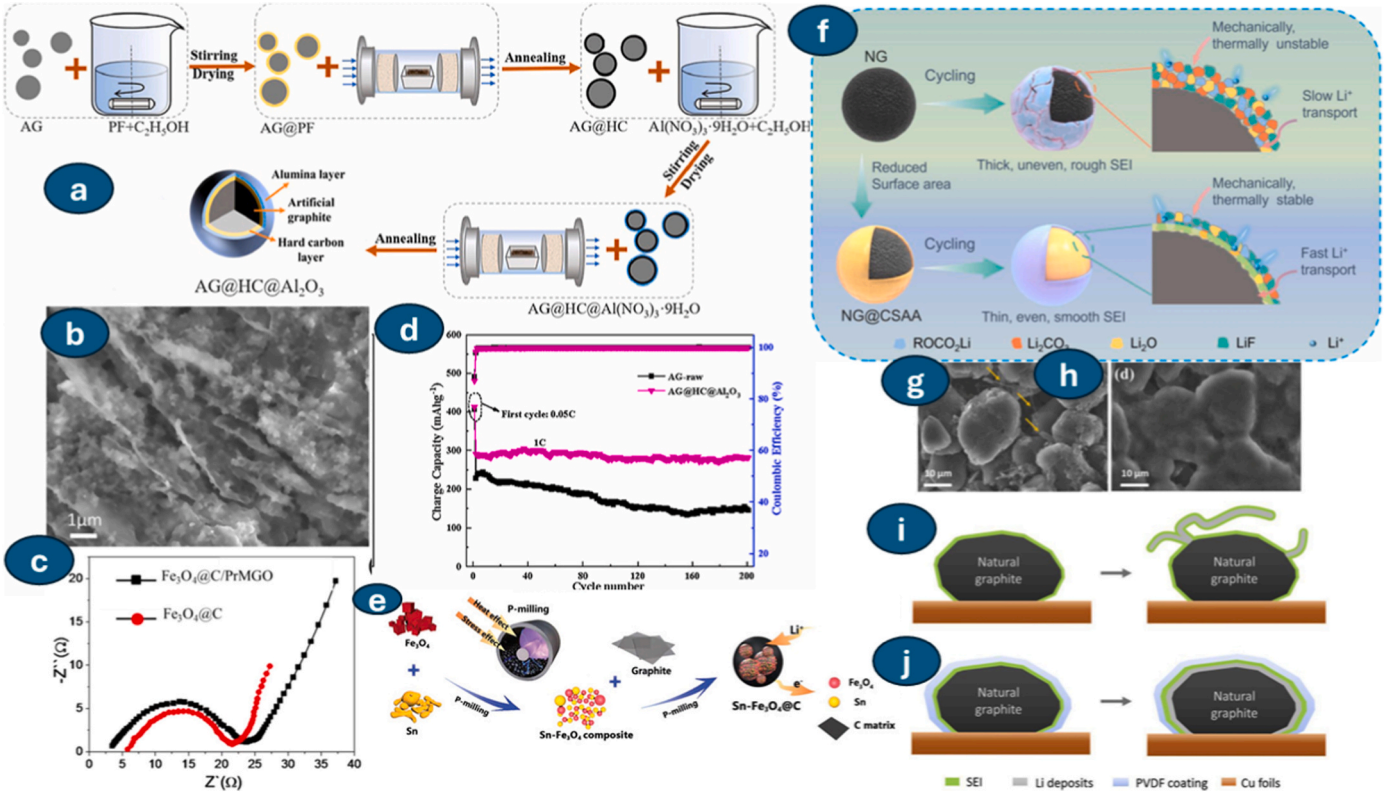

Fig. 8. (**a**) Synthesis process schematic diagram of AG@HC@Al_2O_3 [83] (**b**) SEM image, (**c**) Nyquist plot [84] (**d**) cyclic performance and coulomb efficiency of AG at various compositions [83] (**e**) [85] (**f**) surface engineering on NG [86].SEM analysis of NG (**g**) and PVDF@NG (**h**) electrodes [87] Schematic illustrations of Li plating on an uncoated NG electrode (**i**) and a PVDF coated electrode (**j**) [87].

derived from different waste materials has the properties of an efficient and good electrocatalyst support and therefore has the potential to increase the performance of anode electrode material. Finally, AG@HC@Al_2O_3 anode material was successfully obtained, aiming to identify the optimal sample for electrochemical performance. Hard carbon/alumina double-coated graphite anodes (AG@HC@Al2O3) were examined as anodes in lithium-ion batteries (LIBs). Scanning electron microscopy (SEM) gives information about the surface morphology of the material of interest, Fig. 7b, with the composite still exhibits more obvious layered structure. The electrochemical reaction kinetic of the Fe_3O_4@C NP electrode is like that of the Fe_3O_4@C/PrMGO electrode, or even better, at an early stage. The resistances to charge-transfer and electrochemical reaction of Fe_3O_4@C NPs and Fe_3O_4@C/PrMGO electrodes are only 16 and 20 Ω, respectively, Fig. 8c [83,84].

Additionally, the more vertical slope also indicates the easier and faster diffusion of lithium ions inside the Fe_3O_4@C NP electrode. This phenomenon might be ascribed to the larger specific area and porous structure of Fe_3O_4@C/PrMGO electrodes that leads to higher ionic conductivity. These outcomes are attributed to the negative effects of high-speed synthesis, including inhomogeneous morphology and new SEI formation, which impair the ability to accommodate volume expansion during lithiation and delithiation, which consume lithium ions, LiOH. The challenges in the lithiation and delithiation processes of batteries are due to electrochemically inert alloying phases. Highlights the performance of After 150 cycles at a rate of 1C, it still maintains a reversible specific capacity of 281.3 mAh g^{-1}, noting that optimal cycle performance is achieved with the composite, Fig. 8d. However, the retention rate of AG@HC@Al_2O_3 is as high as 94.4% after 150 cycles at a current density of 1C anode has the most stable cycle life, while AG@HC@Al_2O_3 has almost no change before and after the cycle, which provides a strong proof for its excellent cycle performance. It is noted that larger pores in the composites lead to poor cycle capabilities due to instability and pulverization [83,84].

A study reported the synthesis of a spherical Sn–Fe_3O_4@graphite compound using high-efficiency discharge plasma-assisted milling, shown in Fig. 8e. Based on the above discussion, the functions of chitosan and Acrylic Acid (CSSA) decoration on NG surface are schematically summarised in Fig. 8f. Heterostructure catalysts include a combination of several materials to make a catalyst. Through the collaboration of different components, heterostructure catalysts permit increased kinetics. Firstly, the CSAA decoration layer significantly reduces the specific surface area of NG by covering the ridges and filling the concaves of the surface, which can decrease the contact between graphite and electrolyte and attenuate the interfacial irreversible decomposition of electrolyte. SEM images of the over-lithiated NG and PVDF@NG electrodes. Various scales of dendritic Li deposits were observed on the NG electrode, ranging from large (>100 μm in length), Li deposits spreading across the electrode surface (Fig. 7g) to nano-sized needle-shaped protrusions, Fig. 8h. In the present case, as schematically illustrated in, Fig. 8i and j, while Li dendrite grew on the uncoated NG particles, the interface of heterogeneous catalysts serves as the site of electron transfer and charge redistribution, thus allowing the ability to control the electronic structures at the active site, Li was plated as a thin film between the β-PVDF and the surface of the NG particle, similar to what was previously observed on the PVDF coated Cu and Li substrates [85–87].

Schematic illustration of lithium-ion storage intercalation in graphite layers and surface modification using tin oxide, Fig. 9a. The electron redistribution at the heterostructure interface leads to a strengthened adsorption sites and strengthened at the interface region. Structural analysis of natural graphite could be divided to flake graphite (FG) and microcrystalline graphite (MG) according to its crystal structure. FG possesses a typical layer structure and large graphite crystal stacking within orientation. It shows strong anisotropic property.

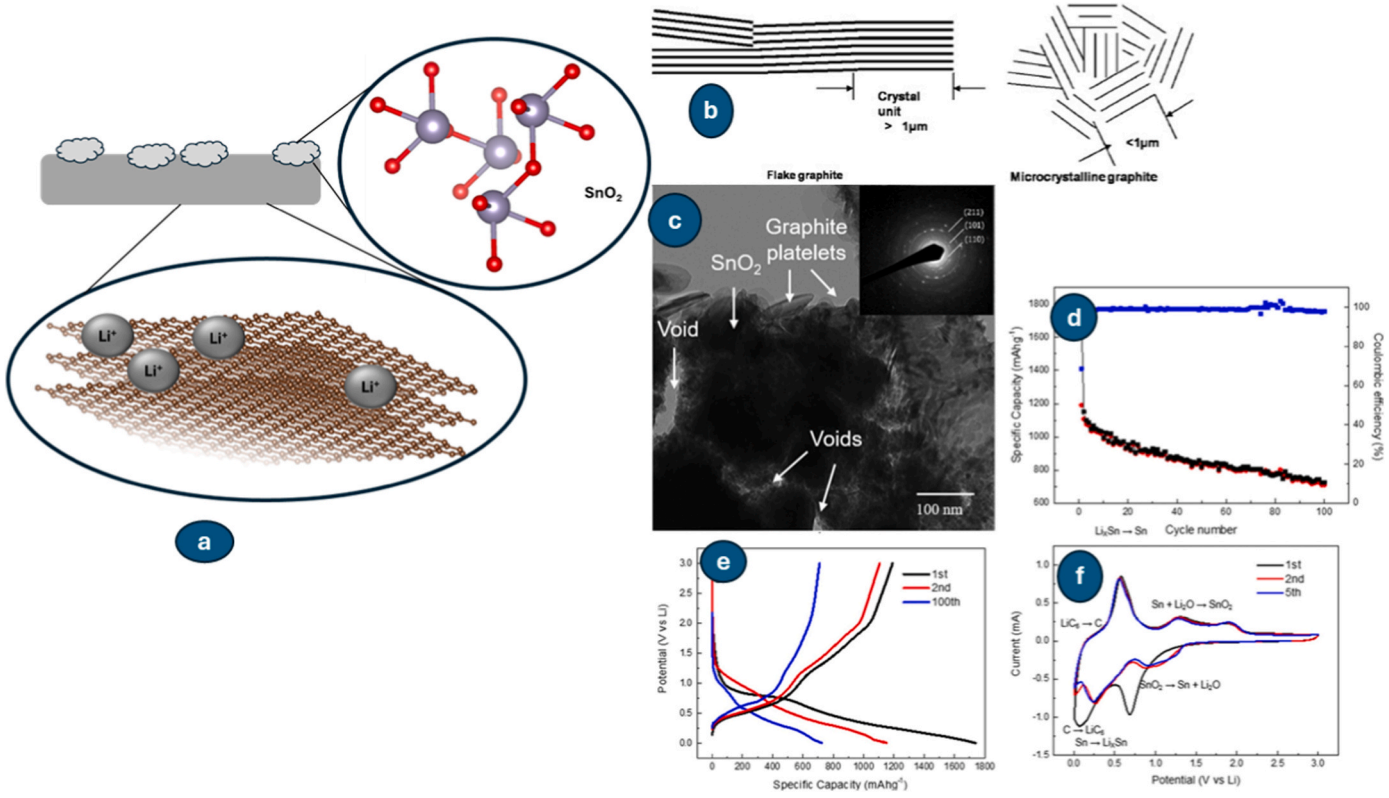

Fig. 9. (**a**) Schematic representation of hierarchical graphite layers (Intercalated Li^+ ions) doped with tin oxide, (**b**) Flake and microcrystalline graphite [88], (**c**) TEM image of graphite nanocomposite [89], (**d**) Cycling performance and coulombic efficiency [89], (**e**) Discharge/charge curves [89], and (**f**) Cyclic voltammograms of graphite nanocomposite. Reproduced with permission from Ref. [89], © 2017 Elsevier Ltd. All rights reserved.

However, MG, which is also called clay-like graphite, is a combination of very small clusters of graphite crystals without order, Fig. 9b. In the realm of improving LIBs to high power and energy batteries, the evolution of novel electrode materials with unique structural designs is of much necessity, such as using SnO_2 as electrode material shown in Fig. 9c. The unique design of SnO_2 presents a high theoretical specific capacity of 1494 $mAhg^{-1}$, which is a promising candidate for the LIBs anode material due to its various engineering strategies, such as morphological modification, dimensional reduction, and the formation of composites. Tragically, most SnO_2-based electrodes are produced using complicated technologies for chemical synthesis, which are not feasible to increase their practical application; furthermore, they are still chronically affected by the consequently poor initial coulombic efficiency and the simultaneously irrecoverable initial capacity loss [88, 89].

Until now to overcome the established irreversible formation of Li_2O by the reactions that occur to fully utilise its specific capacity, this study presents the combination of SnO_2 and graphite using a cost-effective industrial grade high energy ball mill activation to form hierarchical structured SnO_2-C nanocomposites which demonstrate better impressing electrochemical performance electrode with an initial Coulombic efficiency of 68.5% and a reversible theoretical specific capacity of 725 $mAhg^{-1}$ after 100 cycles at current density of 200 mAg^{-1}. This achievement is possible due to the unique structural design which is more on reducing SnO_2 particles to nanostructured range resulting in enhanced efficiency of Li ion diffusion and electron transfer, Fig. 9e, in addition the coating with carbon from nanosized graphite leads to more improved characteristics such as providing a more stable solid electrolyte interphase (SEI) that improves charge transfer on SnO_2 interface to bypass the repeated volume variation and the remaining graphite sheets to prevent SnO_2 agglomeration and pulverization, thus preserving the electrodes integrity, Fig. 9f [89].

Fig. 10a below shows a schematic illustration of the intercalation process of Li in the expanded graphite (EG) based on two models the Rüdorff model for stage I only and Daumas-Hérold model (for stage II, II L, III, IV, and VIII, where 'L' designate a liquid phase that displays no in-plane ordering of Li ions) for various staging the transitions/intercalation. Nevertheless, stages III, IV, and VIII transitions/intercalation in EG30 is thought to be the formation of matching stage compounds such as LiC_{27} (stage III), LiC_{36} (stage IV), and LiC_{72} (stage VIII), justifying the in-plane lithium ordering by LiC_9 packing in the Li^+ intercalated nanosheets of EG30 as per hexagonally close packed diffuse two-dimensional arrays. The high-order staging phenomenon, for example the formation of LiC_{72} as eighth lithium intercalating compounds is like those reported for thin graphite and natural graphite electrodes by Levi et al. [90] and Ohzuku et al. [91], respectively. Additionally, the splitting of stage II into s = II at 0.06 V and s = II L at 0.1 V, is due to the different in-plane lithium orderings by LiC_6 packing densities in EG1, EG10, EG45, and EG60. These results strongly imply that, compared to other EG samples, the turbostratic ordered graphene structures and the shrinkage of the d-spacing of EG30 greatly accelerate the large volume of reversible Li + de/intercalation that periodically generates up to LiC72 as an eighth stage compound. As a result, the results obtained here have been deliberately explained within the frameworks of the EG30 and other EG samples based on the co-existence of the close-packed and hexagonally close-packed diffuse two-dimensional arrays, which are comparable to Daumas-Hérold and Rüdorff cluster models for staged phase transition/staging behaviour.

Fig. 10b, displays the long-term cycling stability of the EG30 and graphite cells rapid charging process, which presents results at different

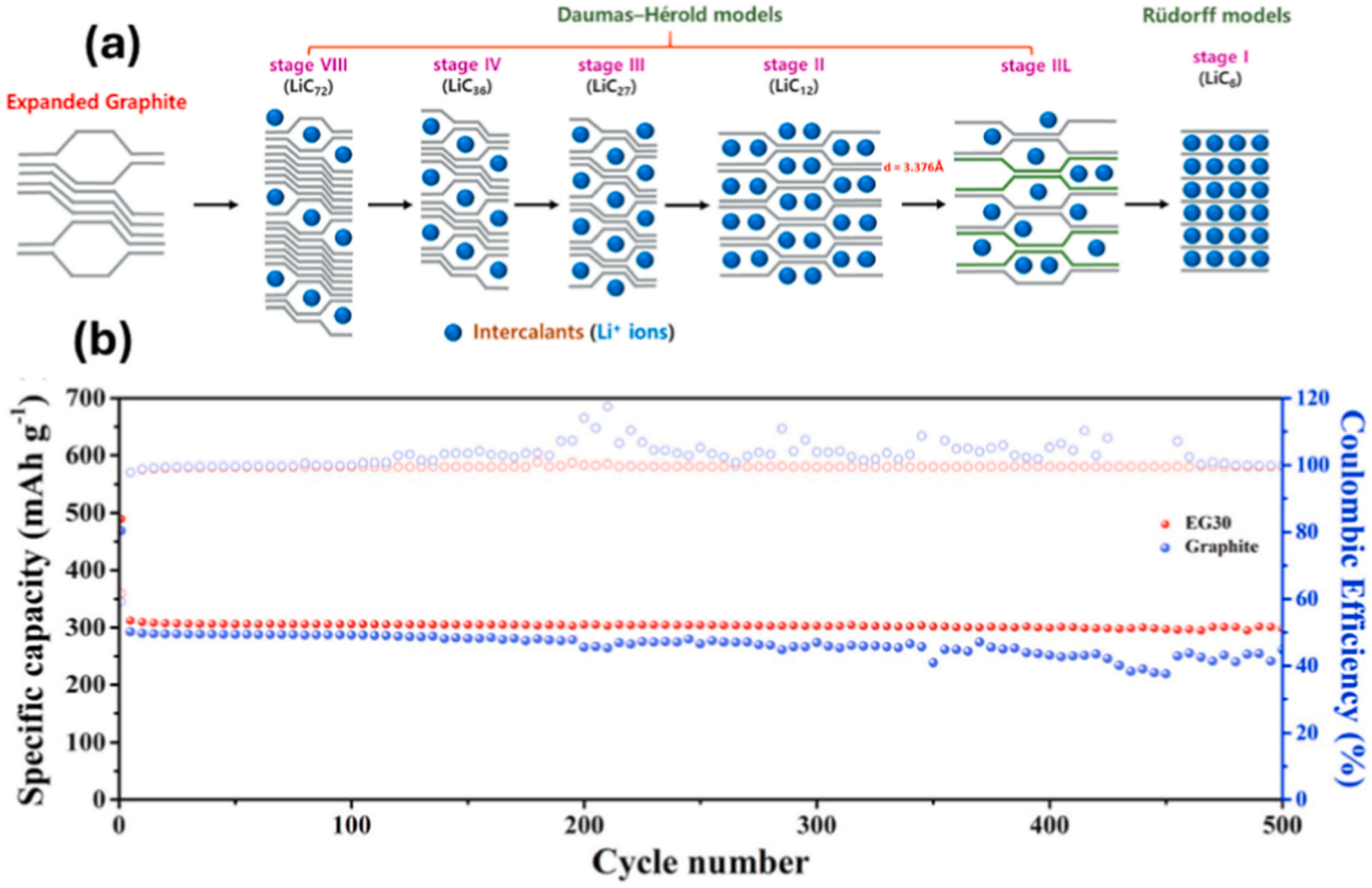

Fig. 10. Illustrates (**a**) lithium intercalating process in expanded graphite, (**b**) cycling stability of charge-discharge profile. Reproduced with permission from Ref. [92], © 2021 Elsevier Ltd. All rights reserved.

current densities for fast charging (lithiation) at 1000 mA g^{-1} and slow charging (delithiation) at 200 mA g^{-1}. The EG30 cell presented much better results than graphite, delivering an initial discharge capacity of ~312 $mAhg^{-1}$ while graphite delivered ~293 $mAhg^{-1}$ and retained ~95.64% of its capacity after 500 cycles. Its capacity remained nearly unchanged, with a low capacity fading rate which was ~0.022% per cycle and excellent stable cycling performance. On the other side, graphite maintained a stable capacity of up to 150 cycles, which was followed by erratic changes in the specific capacity with an unstable CE value up to 500cycles. The distorted charge and discharge curves in graphite during the high-rate electrochemical kinetic reactions are induced by the volume expansion and the shrinkage during the Li-ion insertion/extraction process at a higher charging rates which account for the reported unstable CE which is up to 120% of graphite. These findings indicate that the distribution of lithium storage redox-active sites such as the high ECSA and large BET surface area in the preceding cycles may cause the ultra-quick charging process of the EG30 cell to speed up the fast Li^+ insertion/de-insertion kinetics [92].

The analysis of the synthesized samples for characteristics such the microstructure, other structural properties, and elemental distribution were done using TEM, HRTEM, and EDX shown in Fig. 11 (a, b, c) below. The TEM images confirmed that the synthesized graphite had a porous structure, presenting various pore sizes, but when you comprehensively observe Fig. 11a–c, the pores are not uniformly distributed. These porous characteristics persisted after ABC embedding in PAC was removed during the annealing process, the pores were clustered in some regions, and they were observed sporadically throughout the sample. The pores Improved the surface area between the electrode material and the electrolyte, increasing the Li-ion pathway, which are the enhanced features for a better performance battery [93].

To assess the cycle performance of the PAC-Si-CB-ABC electrode, charge-discharge tests were performed for more than 100 cycles at a current density of 100 mAg^{-1} as shown in Fig. 11. The analysis focused on the general capacity, retention capacity and efficiency of the various binder. With the PAC-Si-CB-ABC and the PVDF binder, the electrodes shown 40% of PAC and 60% of Si which presents a high Si content that exhibited higher capacity than those which shown 85% of PAC and 15% of Si with a low Si content. Nevertheless, the cyclability test presented a slow capacity decay in Fig. 11e. A similar trend on the capacity of the PAC-Si-CB-ABC with the PAA binder, wherein the higher Si content resulted in higher capacity values. When comparing electrodes, the ones with PAA binder presented higher capacity than the ones with PVDF binder, this discrepancy could be due to the conductive medium (CB) in addition to the strong binding between Si and PAA and the porous sites created by the evaporation of ABC. This was particularly noticeable in the samples with greater Si contents, where the PAA binder showed some improvement in performance. As shown in Fig. 11f these improved synergistic effects produce high reversible capacities such as the electrode PAC(25%)-Si(75%)-CB-ABC with PAA binder achieved the highest capacity over 100 cycles, although with slow capacity fading and on the other side the PAC(55%)-Si(45%)-CB-ABC electrode with PAA binder supplied a capacity of 800 mAg^{-1} which maintained 80% of the initial capacity after 100 cycles. When looking into the CE values it was eminent that some fluctuations of CE values occurred demonstrating unstable electrochemical reactions. Albeit the development of large porous sites in the electrode composites led to a high capacity and a reasonable cyclic performance, but further engineering of the structures of the composite electrodes is required [93].

Electrode voltage profiles (a) PAC(40%)-Si(60%)-CB-ABC with PVDF binder, (b) PAC(55%)-Si(45%)-CB-ABC with PVDF binder, (c) PAC (40%)-Si(60%)-CB-ABC with PAA binder, and (d) PAC(55%)-Si(45%)-CB-ABC with PAA binder at a constant current of 100 mAg−1. Fig. 11d shows the schematic representation of the anode's degradation mechanisms at low temperatures. During the first cycles, a primary SEI thin layer with a yellow colour form at the electrolyte and carbon particles interphase to protect the electrode from further corrosion and prevent the electrolyte from breaking down through chemical side reactions. During lithium plating at low temperatures at the interface primary SEI

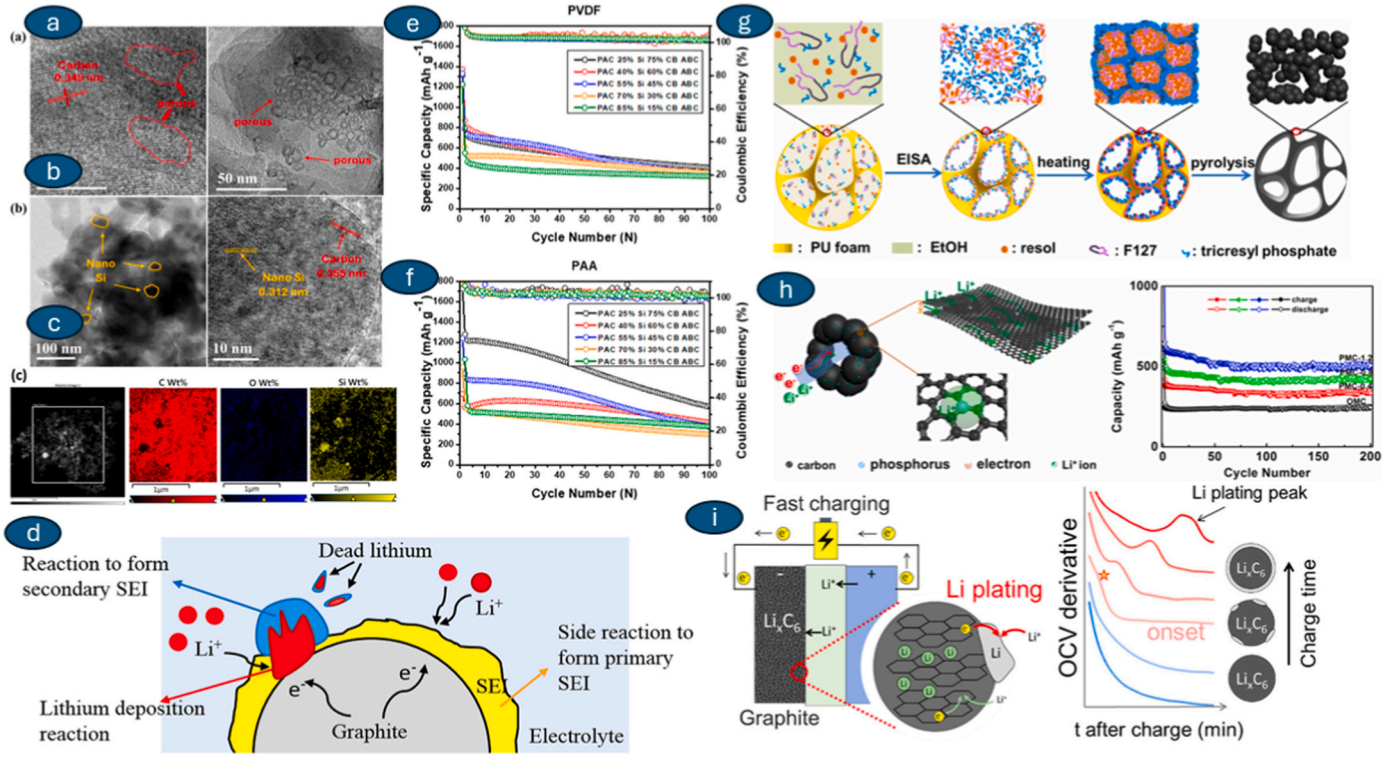

Fig. 11. Illustrates the (**a**) TEM images [93], (**b**) HRTEM images [93], (**c**) EDX images [93], (**d**) degradation mechanism of the anode at low temperatures [74], (**e**) cyclability test [93], (**f**) improved reversible capacities [93], (**g**) schematic mechanism of large pore P-doped mesoporous carbons [94], (**h**) schematics of the P-doped electrode and the reversible charge-discharge peaks [94], and (**i**) schematics of Li plating and the SOC Li plating peaks [95].

produces metallic lithium indicated by red colour and facilitating ion mobility (Li ions) and blocking electrons. The secondary SEI with a blue colour containing the same chemicals as the primary SEI, can be formed when the plated lithium reacts with electrolyte solutions. The formation of the primary SEI, plated lithium, and the secondary SEI occurs under charging [93].

A potential mechanism for the formation of cost-effective large-scale synthesis of P-doped mesoporous carbons is shown in schematic Fig. 11 g. First, the skeletal network of PU foam which serves as an inexpensive and sacrificial substrate, it is impregnated with an ethanol solution containing tricresylphosphate, resol, and F127. It provides numerous interfaces for self-assembly of the meso structure, enabling kilogram-scale synthesis per batch. During the process of evaporating the solvent, tricresyl phosphate can be accommodated into the hydrophobic PPO segment of the F127. In the meantime, because of the strong hydrogen bonding interactions, the resol molecules prefer to be incorporated with the hydrophobic PEO block of Pluronic F127, this strong bonding prevents macrophase separation of the hydrophilic resol and hydrophobic phosphorus precursors, ensuring the formation of the TCP-F127-resol composite micelles. Then the micelles assemble and aggregate on the surface of the PU foam struts. Further fixing of the meso structure can be a result of cross-linking and polymerization of resol during the thermos polymerization process. The different nano-structures in Fig. 10h are responsible for significantly improved electrochemical performance [94,95].

First, the well opened mesoporous framework composed of tiny nanoparticles offers efficient contact with the electrolyte, promotes and creates active sites for lithium storage, these active sites shorten the diffusion distance for Li-ions, and it speeds up the transfer of electrons. For fast-rechargeable, long-lasting Li-ion batteries, P-doped mesoporous carbons with a high P content, large pore size and small domain diameter have been synthesized in a large-massive scale shown in Fig. 11h. The theoretical discharge and charge capacities of PMC-0.4, PMC-0.8 and PMC-1.2 remained around 330, 420 and 500 $mAhg^{-1}$, respectively, after 200 cycles at a current density of 0.5 C, these results were much better than the 242 $mAhg^{-1}$ of the immaculate ordered mesoporous carbon as shown in Fig. 11h. Petzl et al. [96] presented that various analysis of voltage profiles after charging shown quantitative estimation of lithium plating. For a low to medium SOC value, a linear dependence of the plated lithium mass was found; however, a reversible plated lithium was less when charged to a comparatively high SOC [96].

The growth rate and the commencement point of the Li plating were determined using linear regression, but as the temperature decreased, the growth rate increased and the initiation point shifted to a lower SOC, meaning that the plating process started earlier, and this plating-stripping process of lithium at different SOC levels is illustrated in Fig. 11i. At low SOC. lithium is regionally plated with a thick structure, which ensures great electric contact, with the result that the deposition structure at low SOC can therefore be observed as the initial stage of dendrite formation, which continues at medium SOC. Most of the plated Li is therefore stripped, which leads to the remaining challenge for fast charging lithium-ion batteries that is not safe in real-time. This includes identifying the Li plating process at the graphite electrodes, which is a cell component that is commonly known to limit the performance of fast charging (5,6). Lithium ions must be released from the positive electrode and inserted into the graphite negative electrode to allow the LIBs charging process to occur, nevertheless, significant overpotentials and Li-ion concentration gradients form during fast charge, which may lead to the unwanted deposition of Li metal onto the graphite surface, a less known term as lithium plating. In extremely rare cases, plating Li may result in cell shorting that can lead to hazardous thermal runway and electrolyte oxidation. Li plating also causes a short-term capacity loss due to the decrease in cyclable lithium and the increase in cell resistance over-time, as well as short-term efficiency losses due to the poor reversibility of the Li plating/stripping process [94–96].

The material used on the anode electrode is the most crucial for the commercialisation of these batteries. A trend of research presents that graphite is the best mainstream anode material for LIBs because of its cost-effective advantages, a considerable theoretical capacity, and a low lithiation/delithiation potential. Graphite has two main categories, artificial graphite and NG, artificial graphite is produced through carbonization and graphitisation of organic precursors at a very high temperature, which is an expensive and time-consuming production process, and furthermore, the CO_2 and other industrial pollutants generated during these processes do not align with the requirements of carbon neutrality and sustainable development. NG is prepared from carbon-rich organic compounds which are subjected to high temperatures and pressures under geological conditions, and this kind of production consumes significantly lower energy than artificial graphite production. In artificial graphite, the process associated more with energy consumption is the graphitisation method, this process requires heating the precursor material to temperatures higher than 2500 °C, which consumes a substantial amount of energy, with electricity being the main source of energy [97].

However, the production of NG anodes does not consume this much energy because there is no involvement of the graphitisation process, it only concentrates on mining and preliminary processing stages, which consumes less energy leading to lower production costs. As shown in Fig. 12a, one tonne of NG anode requires about 1.1 × 104 MJ of energy to produce, whereas on the other side one tonne of artificial graphite anode requires about 4 × 104 MJ, which is 3,6 times more than that of NG. This different energy consumption of these processes leads to significant variation in the production cost of these anode materials. The CO_2-equivalence (CO_2-eq) emission is lower in NG being 5.3 t while for artificial graphite its over 10 metric tons. In conclusion, the production of an artificial graphite anode is expensive, energy-intensive, and associated with a high carbon emission, while NG anodes offer better sustainability for the environment [97–101].

The carbon nanofiber with an amorphous carbon structure and composed of microcrystalline graphite material in Fig. 12b has a diameter of 200 nm. The insets display the local morphology TEM images and the proposed schematic microstructure of fiber. The CNF is amorphous and made up of several microcrystalline graphite material, in contrast to the bulk graphite that has crystal structure with a carbon layer of loose coupling; hence, the CNF that dissipated during the hydrothermal process is decomposed into microcrystalline graphite, where nickel oxide may act as a catalyst. The microcrystalline graphite is an in-situ composite showing a hexagonal structure of NiO sample, in which it acts as the key role in enhancement of electrochemical properties. Nevertheless, the mechanism of disaggregation of carbon nanofibers is unknown and will be thoroughly examined in future special work [102, 103].

The cycling performance as shown in Fig. 12c further explains the battery cycling stability of the H-NiO sample over the C-NiO. The reversible discharge of H-NiO in the second cycle displays a slight increase with a coulombic efficiency of about 98% and it delivered a high reversible specific capacity of 1111.6 $mAhg^{-1}$ after 45 cycles at a current density of 100 mAg-1. However, the theoretical capacity of C-NiO electrode show very rapid capacity fading during the cycles, which decreases from the initial capacity of 1237.1 to 31 $mAhg^{-1}$ after 45 cycles. The electrical contact between the current collectors and the conductive additives is lost due to the pulverization of the C-NiO samples. The NiO components undergoes pulverization and aggregation during the discharging/charging processes, which causes capacity fading. When it comes to lithiation/delithiation processes, the microcrystalline graphite component shows both chemical and mechanical stability, it is uniformly dispersed in NiO nanoplates within the composite material. Additionally, to its superior electrical conductivity, the microcrystalline graphite in the composite electrode efficiently reduces the NiO component's volume change and pulverization while impeding aggregation in the cycled electrode [102–104].

Sun et al. [83] used a high-energy mechanical milling technique to

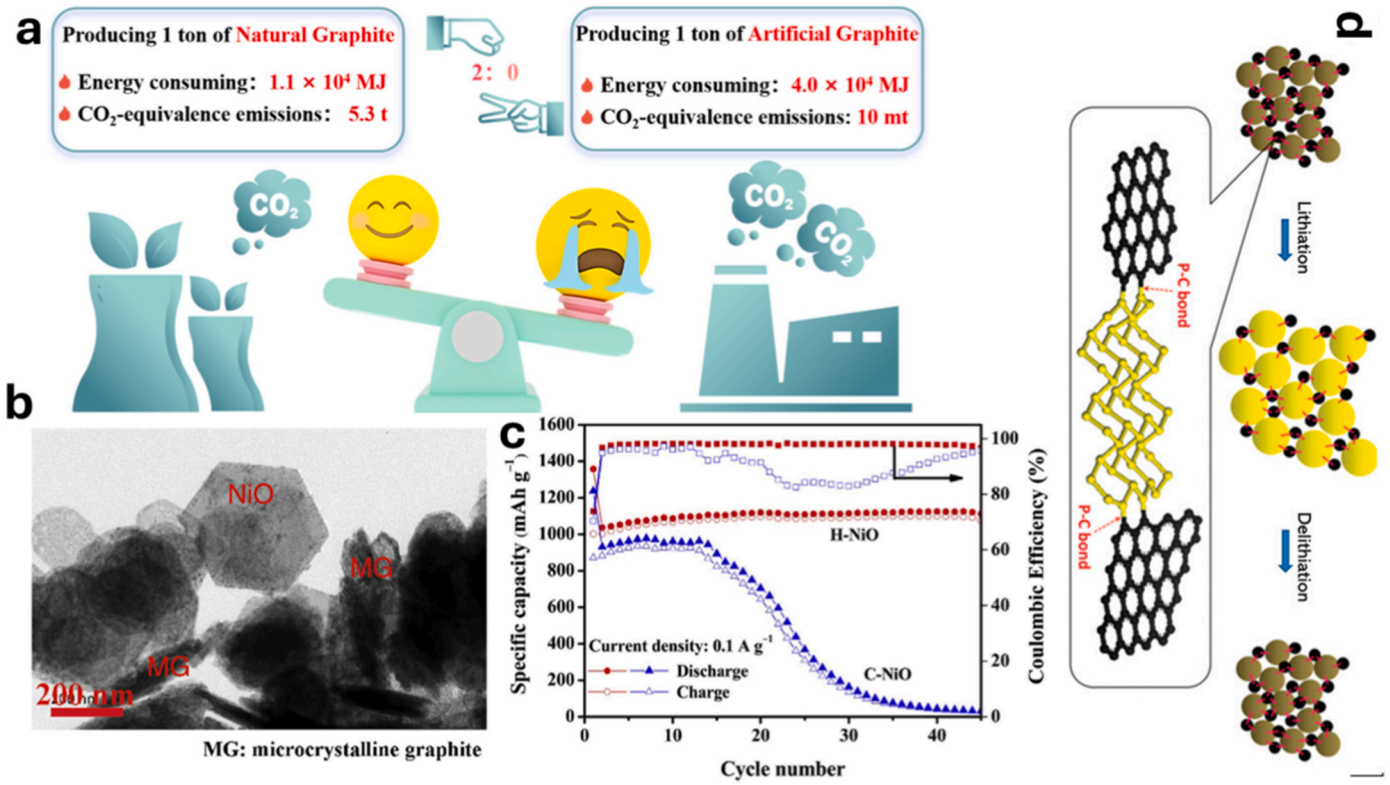

Fig. 12. Showing the (**a**) characteristics of natural and artificial graphite [101], (**b**) TEM images of the amorphous carbon structure and the microcrystalline graphite [102], (**c**) battery cycling stability of the H-NiO over the C-NiO samples [102], and (**d**) schematics of a high-energy mechanical milling process for preparing BP-C composites [103].

prepare a black phosphorous NPs/graphite (BP-G) composite anode with stable P-C bond, which could sustain good electrical contact between phosphorous and graphite for enhancement of electrochemical performance of batteries even after a significant volume change as shown in Fig. 12d. Investigations of BP-derived P-C bonds and various carbon sources such as graphite, carbon black, fullerene and graphite oxides have revealed that the P-C bonds of the BP-Graphite composite are strongest, which is explained by the strong connection bond between the graphite and the phosphorous particles, with the prepared BP-G showing an initial discharge capacity of 2786 $mAhg^{-1}$ at a current density of 0.2 C with 80% capacity retention after 100 cycles [104–108].

2.5. Physicochemical properties

The investigation utilized X-ray photoelectron spectroscopy (XPS) to examine the chemical states of carbon atoms in lignocellulose, L-HC-2500, and L-AG-2500 as shown in Fig. 13a, b, c. The findings revealed core levels of C1 and O1 in all samples, with L-AG-2500 lacking a Fe2p peak, indicating effective removal of iron catalysts after acid washing. The C1s spectra were decomposed into peaks corresponding to various chemical states such as H, sp2, sp3 carbon, and various oxygen-containing groups shown in Fig. 13d-f. The' areal ratios of these peaks were graphed for each sample, showing that lignocellulose comprises a notable amount of oxygen functional groups, particularly H/vacancies. The carbonization and catalytic graphitisation of lignocellulose were shown by decreased oxygen functional groups and the development of sp2 and sp3 carbon structures. Specific carbon ratios sp^3 to sp^2 were reported for L-HC-2500 and L-AG-2500, with L-AG-2500 exhibiting a lower ratio, reflecting its highly crystallised graphite form. This was further evidenced by comparing the C-H/vacancy peak ratios; a lower ratio in L-AG-2500 suggested increased crystallinity due to the iron catalyst's impact. XRD and Raman spectroscopy analyses supported these conclusions. Further elemental analysis verified that L-AG-2500 had a higher carbon content [109,110].

The study employs scanning electron microscopy (SEM) and transmission electron microscopy (TEM) to analyze the morphology of prepared samples as shown in Fig. 13g and h. Findings revealed that carbon coated spherical graphite, when coated, takes on an accordion-like nanosheet structure, and spherical graphite nanosheets exhibit the Tyndall effect in colloidal dispersions following sonication. SEM and TEM images of coated spherical graphite nano are effectively encased within graphite nanosheets, with little agglomeration and minor gaps observed between silicon nanoparticles and nanosheets, Fig. 13(g and h) [57]. The investigation examines the structural traits and interactions in a RP/G compound synthesized through ball milling. This composite contains agglomerated particles of red phosphorus (RP) and graphite, with a uniform distribution of phosphorus and carbon elements shown in Fig. 13i, j. XRD analysis shows that post-milling RP remains amorphous, while graphite loses its crystalline structure, resulting in a broad peak in their combined XRD pattern indicating disorder. HRTEM and Raman spectroscopy support these findings, as Raman spectra reveal weakened RP characteristic bands and a shifted G band of graphite, indicating strong RP-graphite interactions and increased disorder. The higher ID/IG ratio in the Raman spectrum of the compound emphasises considerable structural disorder compared to pure graphite [60,112].

In this research, we examined the structural characteristics of SC, SCNi, and SCNNi samples through the analysis of their XRD and Raman spectra. The XRD analyses indicated the presence of amorphous carbon peaks, characterised by broad diffraction peaks suggestive of minimal graphitisation, which are shown XRD Fig. 13k and l. Raman spectroscopy results demonstrated that variations in treatments did not affect the characteristic peak positions, preserving the D band around 1350 cm^{-1} and the G band near 1580 cm^{-1}. The SC sample without treatment showed the highest degree of graphitisation, reflected by an ID/IG ratio of 0.99, and the introduction of $NiCl_2$ as a template showed little effect on this ratio. The study further explores the SCNNi samples, which

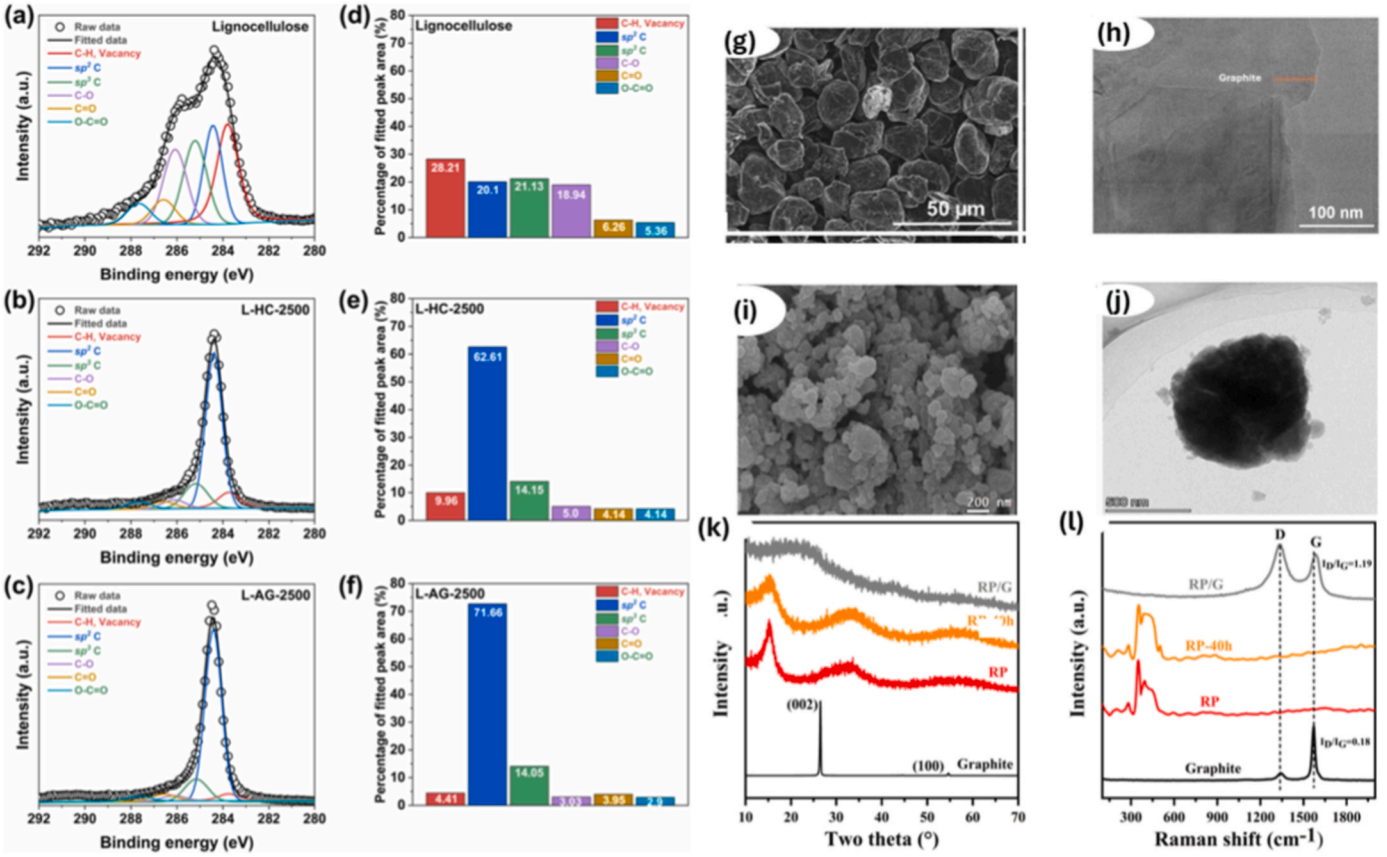

Fig. 13. XPS C1s spectra, after deconvolution, for (**a**) lignocellulose, (**b**) L-HC-2500, and (**c**) L-AG-2500. Relative proportion of the fitted peak areas of C1s components for (**d**) lignocellulose, (**e**) L-HC-2500, and (f) L-AG-2500. [105113], © 2025 Elsevier. (**g**) SEM carbon coated spherical graphite and (**h**) TEM images of carbon coated graphite. Reproduced with permission from Ref. [111], Copyright © 2020 American Chemical Society. (**i**) Images captured by FESEM show the RP/G composite, while (**j**) illustrates the RP/G composite through TEM images and EDS elemental mapping. Part (k) presents the XRD patterns alongside the Raman spectra (**l**) for pristine graphite, RP, RP after 40 h, and RP/G. Adapted with permission from Ref. [60], © 2022 Elsevier.

incorporate both nitrogen doping and nickel as pore-forming agents. The ID/IG ratio of 1.05 indicates a lower level of graphitisation and an increased presence of defects, attributed to more abundant oxygen/nitrogen functional groups and high-temperature pyrolysis. N2 adsorption–desorption measurements provide insights into surface area and pore distribution. The SCNi sample exhibits a type-IV isotherm with a hysteresis loop, indicating a higher abundance of mesopores, whereas the other samples display type-II isotherms with overlapping adsorption and desorption isotherms, pointing to differing pore structures [112, 113].

The research investigates the crystal structures of materials utilising X-ray diffraction (XRD) and Raman spectroscopy. XRD analysis identifies two peaks associated with the 002 and 100 planes characteristic of graphite-like crystals, with interplanar spacing determined via Bragg's equation in Fig. 14a, b. Raman spectroscopy detects D and G peaks, where the I_D/I_G ratio serves as an indicator of material defects. The outcome indicates minimal graphitisation in all samples; however, NT2–1000 and NT3–1000 exhibit higher ID/IG ratios, pointing to more defects, corroborated by XRD data. The interlayer spacings of the T-1000 and NT2–1000 materials are also considered in the context of the Na^+ ion intercalation potential. T-1000's interlayer spacing of 0.362 nm is insufficient for Na^+ insertion, whereas the 0.372 nm spacing of NT2–1000 along with significant nitrogen doping makes it viable for sodium storage, offering ample interlayer space and defects. Fig. 14e, f N_2 adsorption-desorption isotherms show that both materials feature diverse pore sizes, as indicated by Type IV isotherms, with no overlap between adsorption and desorption curves [112–116].

This study employs Raman spectroscopy to analyze the crystallinity of carbon structure by evaluating the degree of disorder, such as structural defects and levels of structural order which are the graphitic content. The intensity ratios of the D and G bands (ID/IG) represent a highly active area and sites that are suitable for the capacitors and supercapacitor, most important for the high-power density. For anode application in sodium-ion batteries NIBs and LIBs, the medium ratio denotes a desirable combination of good power and energy density. The high mechanical strength, high chemical stability, high electrical and thermal conductivity, and high energy density are all benefits of the low ratio on the anode of LIBs. As shown in Fig. 14d, the Raman spectrum displays samples heated at 225 °C with a strong D band at around 1362 cm^{-1} and a G band around 1588 cm^{-1}. The prominent D band indicates high levels of disorder or defects in the carbon structure, which are commonly associated with extremely faulty graphitic carbon or amorphous carbon. Although the intensity of the G band represents some hybridised carbon sp2, the high D/G ratio points to a substantial degree of disorder as shown. The absence of a 2D band at very high wavenumbers such as 2700-3000 cm^{-1} indicates a lack of well-formed graphene-like layers, therefore, at 225 °C the carbon material formed has no graphitic character and is mostly amorphous, as shown in Fig. 14e. The D band is still present in the 275 °C spectrum at about 1372 cm^{-1} but the G band at around 1588 cm^{-1}, it becomes more intense compared to the D band. This indicates that, in comparison to the 225 °Csamples, there is a minor increase in the degree of graphitisation, although defects are still present. Although, it is underdeveloped, a weak 2D band is seen at about 2941 cm^{-1}, suggesting the start of some graphene-like layer production [113–116].

Compared to the 225 °C samples, the D/G ratio is lower, indicating a

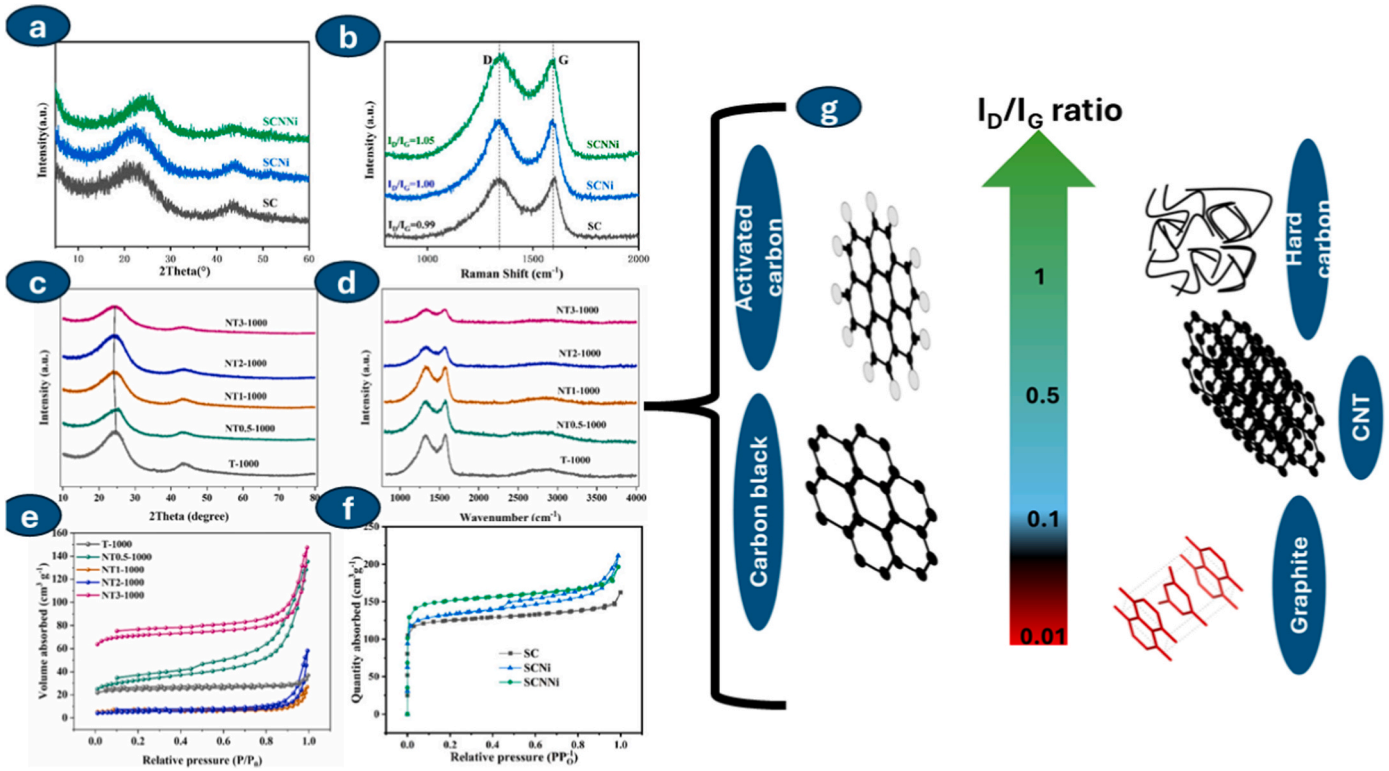

Fig. 14. (**a**) XRD patterns, (**b**) XRD (© 2025 Elsevier). Reproduced with permission from Ref. [113], © 2021 Elsevier (**c**) Nitrogen adsorption-desorption, [114], © 2025 Elsevier). and (**d**) Raman spectra of the SC [86], © 2021 Elsevier). (**e**) BET spectra. Reproduced with permission from Ref. [114], © 2025 Elsevier. (**f**) Nitrogen adsorption–desorption isotherms analysis [113]. (**g**) Schematic of Raman intensity ratios ID/IG ratio.

decrease in structural defects but not enough to categorise the material as completely graphitic. At this temperature, the carbon structure is becoming more graphitic, although it is quite flawed. There is a noticeable improvement in graphitisation in the spectrum at a temperature of 300 °C. The G band at approximately 1586 cm^{-1} is significantly more intense, showing a higher concentration of hybridised sp2 carbon atoms, while the D band at approximately 1365 cm^{-1} is still present, indicating the presence of defects. In addition, a more prominent 2D band, typically of few-layer of graphene or graphitic carbon structures occurs at around 2896 cm^{-1}. The intensity of the 2D band is not that strong more than that of the G band, suggesting that the material is becoming more graphitic, Fig. 14f,g [116].

The lower D/G ratio suggests fewer defects compared to samples at lower temperatures; this shows a higher degree of structural order and the formation of carbon or graphitic material adjacent to graphene, schematic representation Fig. 14g. A distinct trend towards increasing graphitisation may be observed on the path from 225 to 300 °C, the material is primary amorphous carbon with considerable disorder at 225 °C it shows some graphitic tendencies at 275 °C although it still has a lot of disorder. At 300 °C the presence of a strong G band and a visible 2D band suggests the successful preparation of graphite-adjacent or graphitic carbon structures, whereas the flaws are still present. Thus, these spectra illustrate that 300 °C is the best ideal temperature among the three for the synthesis of graphene-adjacent or graphitic carbon structures using nickel nitrate with SCBA [108,117].

The presence of residual organic compounds and the absence of characteristic graphene peak the C=C stretching vibrations around 1580 cm^{-1} indicate the hybridized carbon sp2 in the graphitic material. The persistent O-H and C-H stretching vibrations indicate that the organic materials have not completely decomposed, which prevents the formation of a pure carbon matrix required for graphitisation. According to this analysis, the final product is probably a combination of iron oxides and residual organic compounds along with amorphous carbon. There are inadequate conditions for the full synthesis of the graphene-adjacent material, even if some chemical changes, such as dehydration and iron oxide formation, occur with increasing temperatures. Under the experimental conditions specified, the iron oxides formed are insufficient to catalyze graphitisation, and the carbon remains mainly amorphous, Fig. 14g [118–120].

Table 3below shows properties of anode material precursors that can be used in the anode of Lithium-ion batteries; these precursors present significant differences such as structure, processing conditions, and performance. The well-known graphite offers such as high ICE and its cost-effectiveness, while hard carbon presents excellent cycling stability and more applicability across Li^+, Na^+, and K^+ systems. On the other hand, MOFs and MXenes feature larger tunable surface area and good safety, which makes them useful in many battery chemistries with less limitations, such as lower ICE and being expensive. All these material's properties show their sustainability in the energy storage applications [113,119]– (see Table 4).

Carbon-based functional nano additives are promising electrode components because their highly conductive networks and porous structures promote fast electron transport and excellent high-rate capability, while also enhancing and stabilizing the mechanical integrity of the electrode. Representative materials include graphene, carbon nanotubes, and biochar. Silicon–graphite composites leverage the extremely high theoretical capacity of silicon (~3579 mAh g^{-1}) together with the mechanical durability and outstanding electrical conductivity of graphite, thereby delivering higher energy densities than conventional graphite-only anodes. Approaches to mitigate the ~300% volume expansion of silicon, prolong cycling stability, and preserve robust electrical contact depend strongly on the use of graphite frameworks and carbon coating layers [122–124].

SnO_2-based composites, which offer a theoretical capacity of ~782 mAh g^{-1} via a conversion reaction with lithium, are regarded as attractive anode materials for achieving improved cycling durability and

Table 3
Anode precursor materials in lithium-ion technology featuring distinctive properties [121].

Materials	Graphite	Hard carbon	MOFs	MXenes
Raw materials	Natural graphite/pitch/ petroleum coke	Resin/ pitch/ biomass	Metal ions/ clusters and Organic linkers (ligands)	Transitional Metal carbides
Carbonization temperature	2500–3000 °C	<1500 °C	1000 °C	-
Interlayer distance [nm]	≈0.335	0.37–0.42	≈0.42	0.19- 0.55
True density [g cm^{-3}]	≈2.2	1.4–1.8	0.126	2–4
Expansion rate of electrode (%)	≈10	≈1	-	-
Charge capacity at low temperatures and fast-charging performances	−15 °C/3 C	−50 C/ >10 C	20 °C	−25 °C/<25
Cycling ability	Medium	High	Medium	Medium
ICE	Excellent	Poor	Excellent	Poor
Origin of major capacity	Low-voltage plateau region	Sloping voltage region	Low-voltage plateau region	Low-voltage plateau region
Application specific properties	Li-ion battery	Li/Na/K-ion battery	Li/Na/K -ion battery	Li/Na/K/Zn-ion battery
Safety	Good	Excellent	Good	Excellent
Cost	Low	High	Low	High

rate capability, especially when confined in or combined with conductive graphene or graphite frameworks. In such architectures, the carbon networks originating from graphite serve simultaneously as electron-conducting channels and mechanical buffers, suppressing nanoparticle agglomeration and alleviating the volume variation of SnO_2 [124].

In addition, studies have shown that carbon matrices containing well-dispersed Fe_3O_4 nanoparticles, embedded within their carbon frameworks, undergo conversion-type lithium storage and can deliver high reversible capacities of about 900–1000 mAh g^{-1}, along with superior rate capability, largely dictated by the nanoscale morphology and the efficient conductive carbon network. It has also been reported that artificial SEI layers can suppress electrolyte degradation and enable fast-charging graphite anodes with prolonged cycling stability by stabilizing the electrode–electrolyte interface (see Table 5) [125,126].

3. Structure–property–performance relationships

The outstanding electrical performance of graphite arises from the delocalized π-electron density associated with its nanosheets, which is essential for enabling rapid electron mobility along the basal planes. The formation of extensive conductive networks is governed by its layered sp^2-hybridized structure, and in a nanocomposite matrix, the nanosheets or flakes create interconnected conductive pathways that operate close to the percolation threshold. This behaviour is highly advantageous for electrochemical devices, as it promotes efficient electron transport through the electrode material, significantly lowers internal resistance, and enhances charge transfer efficiency. Owing to this conductive network, energy storage systems benefit from rapid electron movement and conduction between electroactive species in lithium-ion batteries, sodium-ion batteries, and supercapacitors, ultimately leading to higher capacity, improved durability, and high-power density [127–130].

Additionally, the two-dimensional morphology and large specific surface area of graphite make it easy to functionalize its surface and to

Table 4
Comparative summary of electrode composition and their design strategies.

Composite type	Design strategy	Capacity	Rate capability	Cycling stability	Advantages	Challenges	Scalability	Ref
Graphite/Carbon (Biochar, Graphene, CNT)0	Conductive nectwork + porosity engineering	Moderate	Excellent	Good	Improved kinetics, Stable SEI	High surface area, low ICE	High	[120,121]
Graphite/Si	Alloying + buffering matrix	Very high	Moderate	Moderate	High energy density	Volume expansion, ICE loss	Medium	[122–124]
Graphite/SnO	Conversion + interfacial synergy	High	Moderate	Moderate	Synergesitc charge storage	Voltage hysteresis	Medium	[124]
Graphite/Fe3O4	Conversion high reaction	High	Moderate	Moderate	Pseudocapacitive behaviour	Structural degradation	Medium	[125]
Surface engineered Graphite	Artificial SEI	Limited	Excellent	Excellent	Fast charging stability	Coating complexity	High	[126]

Table 5
Graphite nanocomposite anodes compared with advanced anodes in LIBs.

Anode	Theoretical specific capacity (mAh g^{-1})	Key merits	Major challenges	Ref
Graphite	~372	Excellent cycling stability, low cost, mature technology	Moderate capacity	[137, 138]
Transitional metal oxides	600–1000+	High capacity via conversion reactions	Low electrical conductivity, large volume change	[139, 140]
Silicon	~4200	Extremely high theoretical capacity, abundant element	Severe volume expansion (~300%), poor cycle life	[141, 142]
Hard carbon	~250–350	Suitable for sodium-ion batteries, good structural stability	Lower conductivity and rate performance	[143, 144]
Graphite nanocomposites	~400–1200 (composite dependent	Improved conductivity, enhanced capacity, structural buffering	Performance depends on composite architectur	[145, 146]
Mxenes	~200–700 (material-dependent)	High conductivity, tunable surface chemistry	Stability issues, synthesis complexity	[147, 148]

anchor customized active materials such as conductive polymers, sulfides, and metal oxides, see Fig. 15. The resulting hybrid graphite structures provide a variety of electrochemically adjustable active sites that promote rapid ion transport and reversible redox reactions. The mutually interconnected graphite network and hybrid active phases work together to deliver favourable reaction kinetics and long-term cycling stability, so engineering these conductive pathways with nanostructures has driven their increasingly widespread application in next-generation storage electrodes to enhance electrochemical performance [131–133].

3.1. Filler dispersion vs agglomeration effect

The monodispersing or uniform distribution of graphite nanosheets directly influences the overall composition of the composite material. As a result, nanofillers are crucial for forming effective interfacial contact with the host matrix, since a homogeneous dispersion can generate continuous conductive pathways. In addition, the exposure of more active sites with a large surface area enhances ion diffusion and adsorption, which in turn promotes thermal transport, mechanical strength, and higher electrical conductivity. In electrochemical systems, this combination of properties in active materials leads to enhanced capacity values in energy storage devices [134].

However, nanofiller agglomeration in graphite nanosheets frequently occurs due to van der Waals forces between adjacent sheets. This leads to inferior electrochemical performance because active sites become blocked, conductive pathways are reduced, and the surface area is less accessible, see Fig. 16. Such aggregates can also induce localized stress, resulting in mechanical instability and poor cycling behavior. Consequently, strategies such as surface functionalization, the use of dispersing agents, and chemical exfoliation are commonly employed to effectively reduce nanofiller agglomeration in graphite-based composites. Precisely controlling the dispersion of nanofillers is essential to fully exploit the structural advantages and inherent electrical properties of graphite nanomaterials [135].

3.2. Interface engineering in graphite nanocomposites

The interfacial chemistry between graphite and the surrounding matrix plays a decisive role in determining physicochemical properties and overall battery performance. When interfacial interactions between the active phases in the composite are strong, they facilitate both efficient charge transfer and effective mechanical load transfer. Consequently, interface engineering approaches that introduce new surface states capable of binding to polymer matrices, or that enable the anchoring of inorganic nanomaterials, can stabilize the composite structure during prolonged electrochemical cycling. In addition, such engineered interfaces enhance pseudocapacitive behaviour as well as catalytic activity. Collectively, these interface-engineering design principles concurrently optimize the critical processes in graphite-based nanocomposites used for renewable energy applications, see Fig. 17 [136].

4. Comparison with other advanced anodes

Graphite-based anodes remain the benchmark material for commercial lithium-ion batteries due to their excellent structural stability, low cost, and well-established electrochemical performance. However, the growing demand for higher energy density and faster charge–discharge rates have stimulated extensive research into alternative advanced anode materials. Among these, silicon, transition-metal oxides, metal sulfides, and emerging two-dimensional materials have received considerable attention due to their significantly higher theoretical capacities compared with graphite. For example, silicon possesses an exceptionally high theoretical capacity of approximately 4200 mAh g^{-1}, which is nearly an order of magnitude higher than that of graphite (~372 mAh g^{-1}). Similarly, transition-metal oxides such as tin oxide, iron oxide, and cobalt oxide offer higher capacity through conversion or alloying reactions. Despite these advantages, many advanced anode materials suffer from substantial volume expansion during lithiation and delithiation processes, which leads to structural degradation, loss of electrical contact, and poor cycling stability [137–140].

In comparison, graphite nanocomposites provide a balanced combination of stability, conductivity, and improved electrochemical performance. The incorporation of nanoscale additives—including metal oxides, conductive polymers, and other carbon nanostructures—can significantly enhance the intrinsic limitations of conventional graphite by improving ion transport pathways and increasing active surface area. For instance, graphite–metal oxide hybrids can combine the high conductivity and structural stability of graphite with the high capacity of

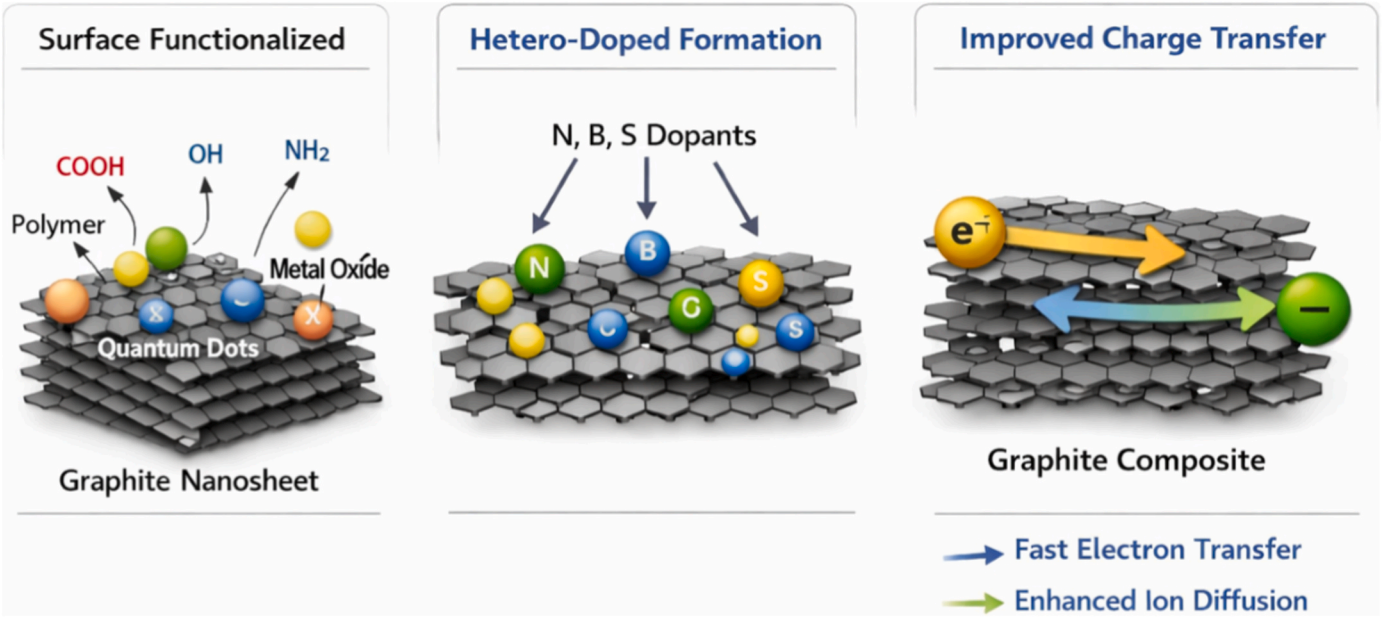

Fig. 15. Schematic illustration showing the formation of conductive pathways in graphite-based nanocomposites and their role in enhancing electron transport and electrochemical performance in energy storage systems.

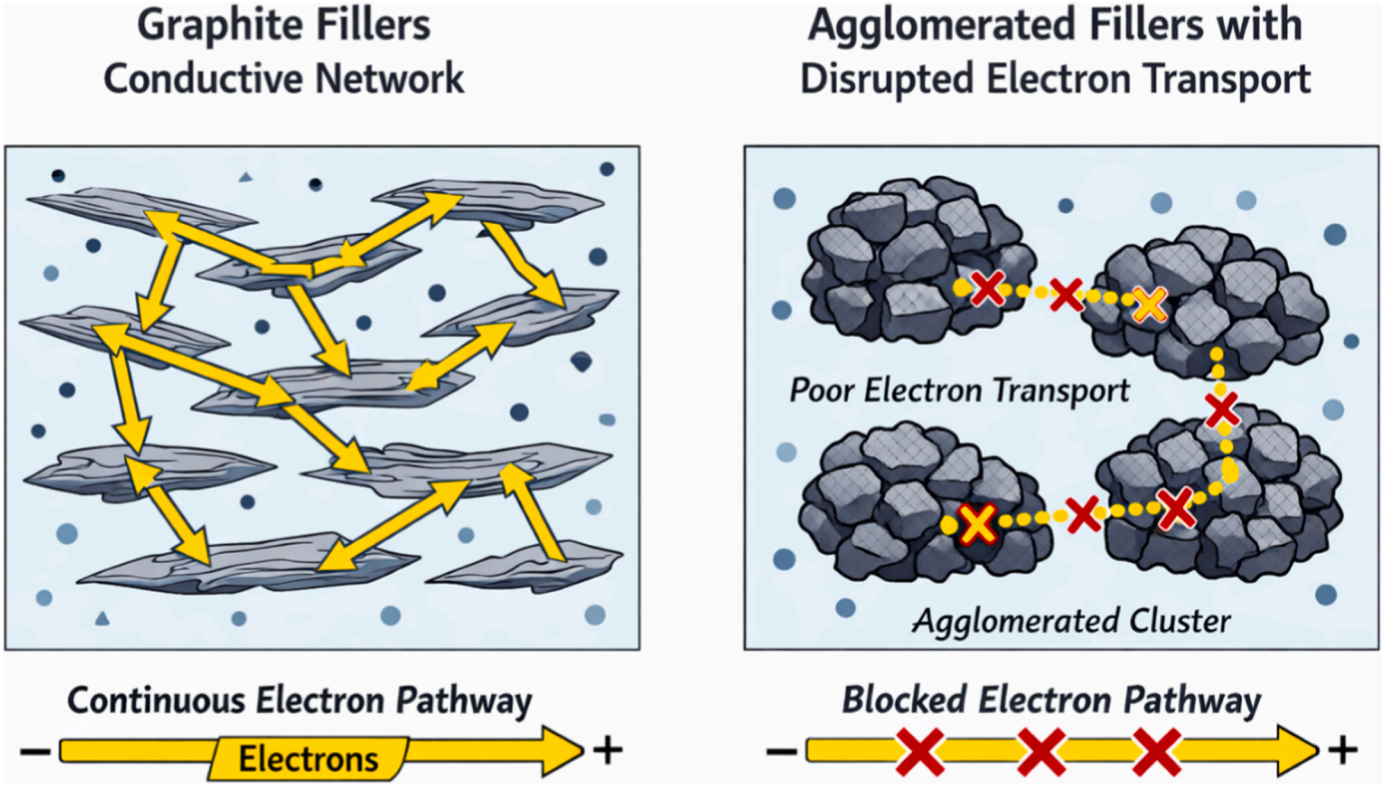

Fig. 16. Comparison between well-dispersed graphite nanofillers forming conductive networks and agglomerated fillers that disrupt electron transport and reduce electrochemical efficiency.

conversion-type materials, resulting in improved reversible capacity and rate capability. Similarly, graphite combined with silicon nanoparticles has emerged as a promising strategy to mitigate the large volume expansion associated with silicon while maintaining a stable conductive framework. These hybrid architectures allow graphite to function as both a mechanical buffer and an electrical network, improving electrode durability and electrochemical efficiency [140–144].

Furthermore, compared with emerging anode materials such as MXenes, hard carbon, and other nanostructured carbons, graphite nanocomposites benefit from well-established processing routes and scalable production methods. While materials such as titanium carbide MXenes or novel alloy-based anodes demonstrate impressive electrochemical performance in laboratory studies, challenges related to synthesis complexity, long-term stability, and cost remain barriers to large-scale implementation. Graphite nanocomposites therefore represent a practical intermediate solution that bridges the gap between conventional graphite and next-generation high-capacity anodes. By integrating graphite with advanced nanomaterials through rational composite design, it is possible to achieve improved capacity, enhanced cycling stability, and better rate performance while maintaining the reliability required for commercial energy storage systems [147,148].

5. Emerging systems: sodium- and potassium-ion batteries

Emerging systems beyond lithium technology is sodium and potassium ion technologies which have attracted researchers worldwide as alternative energy storage technologies given their natural abundance and low cost of sodium and potassium resources. With considerations for grid level storage and renewable energy incorporation they are promising, although their larger ionic radii as compared to Li possess a thermodynamically challenging problem for traditional graphite anodes, as they do not intercalate in graphite thus leading to poor electrochemical performance such as poor cycling stability and very low capacity. Therefore, to overcome these challenges new structural designs are required to engineer high-capacity anode materials capable of accommodating larger ionic radii alkali ions, with tunable expanded interlayer spacing, defect engineering and structural modification [149].

Recently it has been reported graphite hybridization with heteroatom doping, porous carbon and metal compounds significantly facilitate fast ion transport and diffusion, kinetics and storage capabilities in these emerging technologies. Moreover, graphite nanocomposites combined with hard carbon, conductive polymers and metal oxides in sodium ion technology have exhibited improved sodium storage performance by making available more adsorption sites and promote pseudocapacitive contribution, similarly in potassium ion technology relatively low redox potential of K^+/K and favourable ion transport kinetics can enable high power capability when graphite is integrated within conductive composite frameworks. These advances suggest that rationally designed graphite nanocomposites may play a crucial role in enabling high-performance anodes for next-generation sodium- and potassium-based energy storage technologies, particularly for sustainable and large-scale applications [150].

6. Challenges, limitations and outlook

Given significant progress in the field graphite nanocomposites anodes for advanced energy storage systems several issues still hinder their widespread adoption. One notable issue is the low theoretical capacity graphite compared to metal alloy or silicon-based anodes. These composites can improve the capacity and rate capabilities however they introduce complex issues such as interfacial degradation, electrode polarization during prolonged cycling and structural instability. Additionally, volume expansion associated with these anodes often lead to conductive networks, loss of electrical contact and particle pulverization over repeated charge discharge cycles.

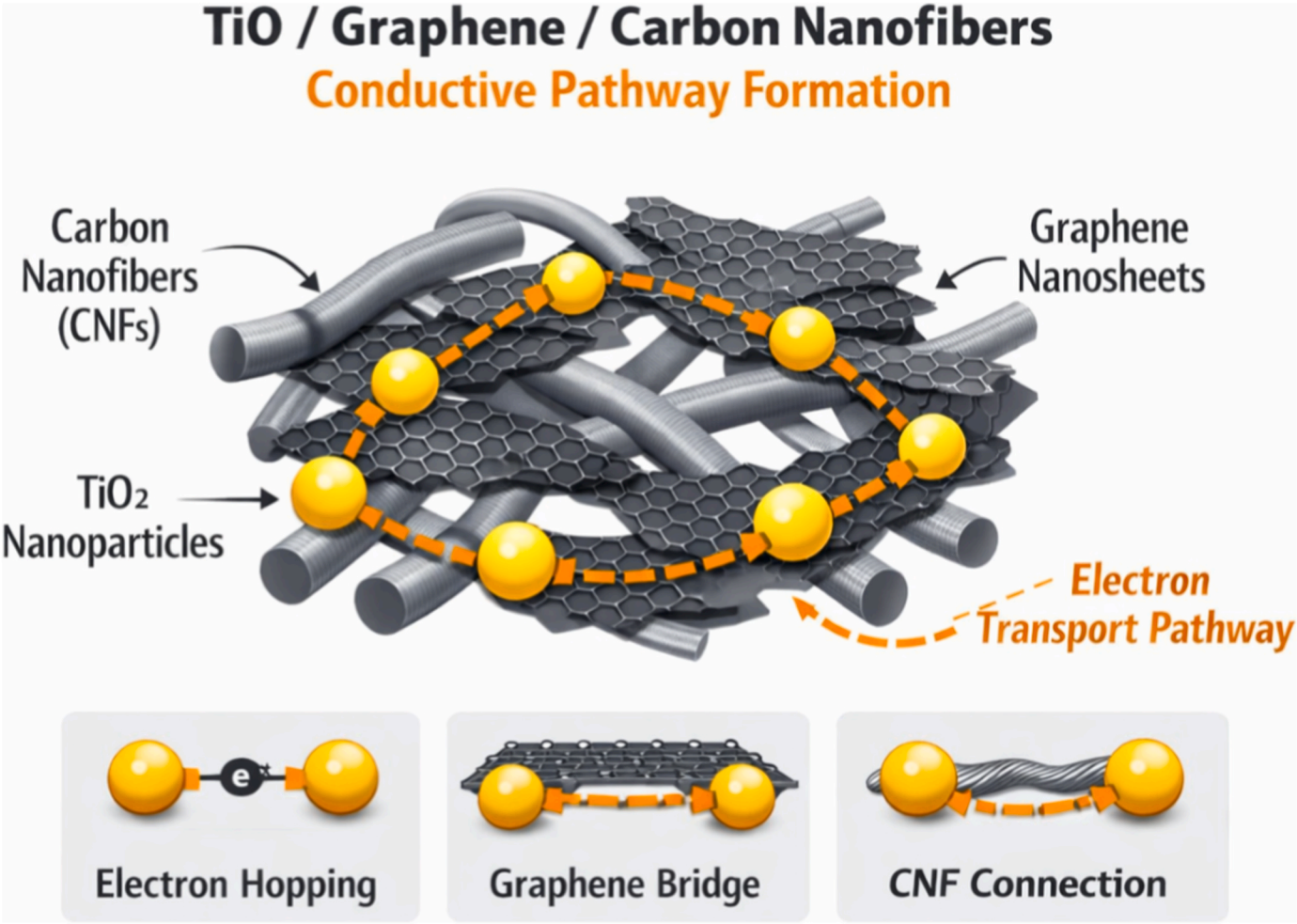

Fig. 17. Schematic representation of interface engineering strategies in graphite nanocomposites showing functionalization, heterostructure formation, and improved charge transfer across interfaces.

Most prominent challenge facing graphite anodes is uniform dispersity and stable interfaces within graphite nanocomposites. Thus, uncontrolled SEI possess a major limitation if not controlled because it plays a major role in long term cycling performance, with many available advanced techniques including hydrothermal, chemical vapor deposition, and template assisted methods may involve high energy intensive, and complex procedures with large scale production considerations, may pose major challenges for industrial scale production. Hence future research should focus on rational chemical designs to optimize structural and interface chemistry of graphite nanocomposites, moreover development porous and hierarchical composite structures can improve the ion diffusion pathways while buffering volume expansions during charging and discharging processes.

Notably advanced techniques to study real time dynamic structural changes during electrochemical processes such as operando spectroscopy or microscopy will play a critical role in understanding these processes, giving valuable insight into mechanistic data for designing stable and efficient nanocomposite systems. Finally, environmentally begnin synthetic procedures should be the cornerstone of practical applications in commercial applications. For the large-scale production of graphite nanocomposites green synthetic methods, low-cost precursor materials and facile fabrication processes should be prioritized. In parallel machine learning and computational modelling learning techniques can streamline and accelerate the discovery of optimized compositions and predictions of structure property relationship performance thus guiding experimental design. These research efforts will aid researchers to potentially understand the knowledge gap between graphite nanocomposites and emerging high-capacity materials, promoting high performance, safe and sustainable energy storage technologies.

6.1. *Rational interface design for fast charging*

The core chemical design is focused on enabling fast charging capability, which is becoming increasingly critical for electric vehicles. From a future research standpoint, it will be advantageous to deliberately engineer ionically conductive interphases and mechanically robust structures to suppress lithium plating under high current densities. Such chemical design strategies should explore graded conductivity architectures, artificial SEI layers with high lithium affinity or ionic conductivity, and lithiophilic surface modifications to lower nucleation barriers.

6.2. *Data-driven and computational materials discovery*

Scalable composite architectures can be rapidly advanced within a relatively short development time through computational screening, made possible by combining density functional theory, machine learning, and phase-field modelling. Together, these tools enable the prediction of tailored Li adsorption energies, support the optimization of composite ratios, and allow the simulation of stress evolution during electrochemical cycling.

6.3. Scalable and sustainable manufacturing

Biomass conversion for energy storage represents a promising niche application; however, the required processing temperatures demand extensive low-temperature treatment of various biomass-derived precursors. For large-scale production, spray drying and roll-to-roll compatible fabrication will support sustainable feedstock use and address scalability needs, both of which will be essential for successful commercialisation.

6.4. Extension to sodium- and potassium-ion systems

Graphite is still the leading commercial anode material in lithium-ion batteries because lithium can form intercalation compounds, reversibly inserting and extracting within graphite layers. In contrast, the larger ionic radius and slower diffusion of sodium, as well as the behavior of potassium ions, demand alternative structural design approaches to address the structural instability and thermodynamically unfavorable kinetics observed in graphite. As a result, materials such as hybrid graphite–hard carbons with expanded interlayer spacing or biogenic carbons are emerging as promising candidates for next-generation energy storage systems.

7. Conclusion

The study demonstrated that graphite nanocomposites and biomass-derived carbon are crucial as anode electrode materials in LIBs. It focuses on key aspects of lithium-ion intercalation into graphite, examining the influence of biochar, heteroatom doping, and graphite nanocomposite modifications on overall battery performance. The growing demand for renewable and alternative energy sources, driven by declining fossil fuel reserves and the impacts of climate change, has intensified interest in biomass. Biomass stands out as a promising energy resource due to its abundance, renewability, and carbon-neutral characteristics. Composed of organic matter from plants and animals, it is particularly suitable for structural sustainable and tunability. This work investigates graphite nanocomposites as an anode material, capitalizing on the high electrical conductivity of graphite channels and the biocompatibility of biochar to enhance the performance of graphite-based anodes in lithium-ion battery electrodes. The research places strong emphasis on physico-chemical parameters that govern charge storage, such as reaction kinetics and the solid–electrolyte interphase, with particular attention to optimizing electrical conductivity. Two-dimensional layered nanomaterials exhibit excellent electronic conductivity and mechanical strength, making them especially attractive for energy storage systems. Hierarchical biochar produced via chemical activation, thermal activation, and heteroatom doping is recognized for its capacity to improve electrode conductivity, thanks to its enlarged surface area and increased interlayer spacing. Ongoing research and development on biochar production methods, including both chemical and thermal activation, have yielded biochar-based anodes with improved performance and methodology. To enable large-scale production and practical implementation, further research is needed to upgrade biochar to battery-grade quality. Additionally, to support industrial-scale deployment, challenges related to raw material sourcing and processing must be addressed so that biochar–graphite nanocomposites can be widely adopted as a low-cost, environmentally friendly electrode material in LIB applications.

Declaration of competing interest

The authors declare that they have no known competing financial interests or personal relationships that could have appeared to influence the work reported in this paper.

Acknowledgments

This research was supported by the Electrochemical Energy Technology Research Group, the Energy Centre, at the CSIR. The financial assistance of the National Research Foundation (NRF) is hereby acknowledged.

Data availability

Data will be made available on request.

References

[1] Shi M, Song C, Tai Z, Zou K, Duan Y, Dai X, Sun J, Chen Y, Liu Y. Coal-derived synthetic graphite with high specific capacity and excellent cyclic stability as anode material for lithium-ion batteries. Fuel 2021;292:120250.
[2] Arnaiz M, Canal-Rodríguez M, Carriazo D, Villaverde A, Ajuria J. Enabling versatile, custom-made lithium-ion capacitor prototypes: benefits and drawbacks of using hard carbon instead of graphite. Electrochim Acta 2023;437:141456.
[3] Shi J, Ehteshami N, Ma J, Zhang H, Liu H, Zhang X, Li J, Paillard E. Improving the graphite/electrolyte interface in lithium-ion battery for fast charging and low temperature operation: fluorosulfonyl isocyanate as electrolyte additive. J Power Sources 2019;429:67–74.
[4] Julien CM, Mauger A. Fabrication of Li4Ti5O12 (LTO) as anode material for Li-Ion batteries. Micromachines 2024;15(3):310.
[5] Zhong H, Liu D, Yuan X, Xiong X, Han K. Advanced micro/nanostructure silicon-based anode materials for high-energy lithium-ion batteries: from liquid-to solid-state batteries. Energy Fuel 2024;38(9):7693–732.
[6] Ankathi SK, Bouchard J, He X. Beyond tailpipe emissions: life cycle assessment unravels battery's carbon footprint in electric vehicles. World Electr Vehic J 2024;15(6):245.
[7] He B, Zheng H, Tang K, Xi P, Li M, Wei L, Guan Q. A comprehensive review of lithium-ion battery (LiB) recycling technologies and industrial market trend insights. Recycling 2024;9(1):9.
[8] Robinson B, Yang J, Tan R, Alekseev S, Low CTJ. Rethinking the roles of graphite and graphene in lithium-ion batteries from environmental and industrial perspectives. Carbon Energy 2025:e70099.
[9] Asenbauer J, Eisenmann T, Kuenzel M, Kazzazi A, Chen Z, Bresser D. The success story of graphite as a lithium-ion anode material–fundamentals, remaining challenges, and recent developments including silicon (oxide) composites. Sustain Energy Fuels 2020;4(11):5387–416.
[10] Shellikeri A, Watson V, Adams D, Kalu EE, Read JA, Jow TR, Zheng JS, Zheng JP. Investigation of pre-lithiation in graphite and hard-carbon anodes using different lithium source structures. J Electrochem Soc 2017;164(14):A3914.
[11] Yadav CS, Azad I, Khan AR, Singh P. Carbon allotropes: past to present aspects. In: Biosensors based on graphene, graphene oxide and graphynes for early detection of cancer. CRC Press; 2025. p. 1–23.
[12] Wu TT, Ting JM. Preparation and characteristics of graphene oxide and its thin films. Surf Coating Technol 2013;231:487–91.
[13] Huang H, He P, Huang T, Hu S, Xu T, Gu H, Yang S, Song L, Xie X, Ding G. Electrochemical strategy for flexible and highly conductive carbon films: the role of 3-dimensional graphene/graphite aggregates. ACS Appl Mater Interfaces 2018;11(1):1239–46.
[14] Aditya DS, Nataraj SK. Structural, optical, and electronic properties of two-dimensional nanomaterials. Two-Dimensional Nanomaterials-Based Polymer Nanocomposites: Processing, Properties and Applications 2024:167–94.
[15] He L, Wei S, Zhang X, Wang S, Xia Y, Ni Z, Li C, Dong W, Shen D, Yang S. Research progress on high-rate graphite anode materials for lithium-ion batteries. J Energy Storage 2025;111:115426.
[16] Goodenough JB, Kim Y. Challenges for rechargeable Li batteries. Chem Mater 2010;22(3):587–603.
[17] Kang S, Ma G, Liu Y, Wang D, Zhang Y, Li J, Xu C, Li Y. Progress in fast-charging graphite anodes for lithium-ion batteries: reaction kinetics. Energy Storage Mater 2025:104531.
[18] Weng S, Yang G, Zhang S, Liu X, Zhang X, Liu Z, Cao M, Ateş MN, Li Y, Chen L, Wang X. Kinetic limits of graphite anode for fast-charging lithium-ion batteries. Nano-Micro Lett 2023;15:215 [online].
[19] Tu S, Zhang B, Zhang Y, Chen Z, Wang X, Zhan R, Ou Y, Wang W, Liu X, Duan X, Wang L. Fast-charging capability of graphite-based lithium-ion batteries enabled by Li3P-based crystalline solid–electrolyte interphase. Nat Energy 2023;8(12):1365–74.
[20] Fu K, Li X, Sun K, Yang H, Gong L, Tan P. Tuning the electrochemical performance of graphite electrodes in lithium-ion batteries: thermodynamics versus kinetics. J Power Sources 2024;606:234568.
[21] Xu K, Lee U, Zhang S, Allen JL, Jow TR. Graphite/electrolyte interface formed in LiBOB-based electrolytes: I. Differentiating the roles of EC and LiBOB in SEI formation. Electrochem Solid State Lett 2004;7(9):A273–7.
[22] Wang X, Hu B, Cao X, Huang S, Xu J, Ge S, Ding J. Edge-engineered graphite modulates SEI formation and enables fast-charging lithium-ion batteries. Chem Eng J 2026:173048.

[23] Febrian R, Septiani NLW, Iqbal M, Yuliarto B. Recent advances of carbon-based nanocomposites as the anode materials for lithium-ion batteries: synthesis and performance. J Electrochem Soc 2021;168(11):110520.
[24] Kim KO, Park SH, Chun HB, Lee WY, Jang BY, Kim D, Yu JH, Yun KS, Kim J, Li OL, Han YJ. Design and optimization of composite cathodes for solid-state batteries using hybrid carbon networks with facile electronic and ionic percolation pathways. ACS Appl Mater Interfaces 2023;15(30):36748–58.
[25] Rocky MRI, Nulu V, Sohn KY. Electrochemical performance of N-doped graphite@ carbon/red phosphorous composite for lithium-ion secondary batteries. Kor J Chem Eng 2025;42(8):1693–704.
[26] Wu H, Wei L, Li W, Shi C, Yao X, Fu Q, Li H, Guo X. Highly conductive carbon/carbon composites as advanced multifunctional anode materials for structural lithium-ion batteries. Adv Funct Mater 2024;34(40):2403729.
[27] Aghamohammadi H, Torabian M. Advances in 3D Si-graphene nanocomposites for Li-ion battery anodes with enhanced stability and rate capability. Particuology 2026;111:303–26.
[28] Liang J, Wang W, Yang W, Zhang Z, Zhang X, Jung Y, Dong X. Facile synthesis of ceramic SiC-based nanocomposites and the superior electrochemical lithiation/delithiation performances. Mater Chem Phys 2020;243:122618.
[29] Kalidas N, Riikonen J, Xu W, Lahtinen K, Kallio T, Lehto VP. Cascading use of barley husk ash to produce silicon for composite anodes of Li-ion batteries. Mater Chem Phys 2020;245:122736.
[30] Haluska O, Meščeriakovė SM, Murashko K, Meščeriakovas A, Kalidas N, Rantanen J, Liu L, Salami A, Lappalainen R, Lähde A, Lehto VP. Production of graphitic carbons from plant-based SiC/C nanocomposites for Li-ion batteries. Mater Chem Phys 2023;296:127286.
[31] Maddipatla R, Loka C, Lee KS. Exploring the potential of carbonized nano-Si within G@ C@ Si anodes for lithium-ion rechargeable batteries. ACS Appl Mater Interfaces 2023;15(50):58437–50.
[32] Han XY, Zhao DL, Meng WJ, Yang HX, Zhao M, Duan YJ, Tian XM. Graphene caging silicon nanoparticles anchored on graphene sheets for high performance Li-ion batteries. Appl Surf Sci 2019;484:11–20.
[33] Li Z, Han M, Yu P, Wu Q, Zhang Y, Yu J. Si-C nanocomposites supported on vertical graphene sheets grown on graphite for fast-charging lithium ion batteries. J Energy Storage 2023;67:107582.
[34] Wang X, Yang M, Zeng T, Xie Y, Wu F, Xie D, Mei Y, Ding Y, Feng D. Unveiling the potential of Bi/FeS-G nanocomposites: a pioneering approach to dual-functional anodes for high-performance lithium-ion and sodium-ion batteries. Ind Eng Chem Res 2025;64(3):1825–36.
[35] Lin HF, Jiang ZX, Chang CT, Yu LJ, Wu YX. Metal oxide-coated graphite composites as high-performance anode materials for lithium-ion batteries. J Appl Electrochem 2026;56(1):16.
[36] Itahara H, Matsubara M, Takahashi N, Kosaka S, Shibata M, Takatani Y. Tin oxide/graphite nanocomposite prepared from the negative graphite electrode of spent Li-ion batteries via a potentially sustainable synthesis method. Chem Lett 2025;54(6):upaf113.
[37] Zhang L, Ding Y, Jin H, Zeng T. MnS/SnS nanocomposite anchored on graphite layers for lithium-ion battery anodes. J Energy Storage 2025;132:117837.
[38] Xu K. Electrolytes and interphases in Li-ion batteries and beyond. Chem Rev 2014;114(23):11503–618.
[39] Cao B, Du M, Guo Z, Liu H, Yan C, Chen A, Chen X, Tang C, Huang JQ, Zhang Q. The future of carbon anodes for lithium-ion batteries: the rational regulation of graphite interphase. Carbon Future 2024;1(3):9200017.
[40] Zhao D, Ding M, Tao M, Shan P, Lin H, Chen Y, Chen J, Zhou Y, Yang Y. Advanced interfacial engineering of graphite anodes for next-generation lithium-ion batteries. Small 2026;22(4):e12150.
[41] Han B, Li X, Bai S, Zou Y, Lu B, Zhang M, Ma X, Chang Z, Meng YS, Gu M. Conformal three-dimensional interphase of Li metal anode revealed by low-dose cryoelectron microscopy. Matter 2021;4(11):3741–52.
[42] Fedorov RG, Maletti S, Heubner C, Michaelis A, Ein-Eli Y. Molecular engineering approaches to fabricate artificial solid-electrolyte interphases on anodes for Li-ion batteries: a critical review. Adv Energy Mater 2021;11(26):2101173.
[43] Sun X, Liu H, Ren KF, Tang WB, Guo C, Bao W, Yu F, Cheng XB, Li J. Understanding the coupling mechanism of intercalation and conversion hybrid storage in lithium–graphite anode. Small 2024;20(35):2401675.
[44] Mohammed LJ, Omer KM. Carbon dots as new generation materials for nanothermometer. Nanoscale Res Lett 2020;15(1):182.
[45] Tripathy S, Rodrigues J, Shimpi NG. Top-down and Bottom-up approaches for synthesis of nanoparticles. Nanobiomaterials Perspect Med Appl Diagn Treat Dis 2023;145:92–130.
[46] Bhagabati P, Rahaman M, Bhandari S, Roy I, Dey A, Gupta P, Ansari MA, Dutta A, Chattopadhyay D. Synthesis/preparation of carbon materials. Carbon-Cont Polym Compos-Containing Polymer Composites 2019:1–64.
[47] Yang X, Zhu P, Ma X, Li W, Tan Z, Sha J. Graphite-like polyoxometalate-based metal–organic framework as an efficient anode for lithium ion batteries. CrystEngComm 2020;22(8):1340–5.
[48] Jayaramulu K, Mukherjee S, Morales DM, Dubal DP, Nanjundan AK, Schneemann A, Masa J, Kment S, Schuhmann W, Otyepka M, Zboril R. Graphene-based metal–organic framework hybrids for applications in catalysis, environmental, and energy technologies. Chem Rev 2022;122(24):17241–338.
[49] Uflyand IE, Naumkina VN, Zhinzhilo VA. Nanocomposites of graphene oxide and metal-organic frameworks. Russ J Appl Chem 2021;94(11):1453–68.
[50] Salimi P, Norouzi O, Pourhosseini SEM. Two-step synthesis of nanohusk Fe3O4 embedded in 3D network pyrolytic marine biochar for a new generation of anode materials for lithium-ion batteries. J Alloys Compd 2019;786:930–7.
[51] Panwar NL, Pawar A. Influence of activation conditions on the physicochemical properties of activated biochar: a review. Biomass Convers Biorefinery 2022;12(3):925–47.
[52] Zielińska M, Bułkowska K. Agricultural wastes and their By-Products for the energy market. Energies 2024;17(9):2099.
[53] Escudero-Curiel S, Giráldez A, Pazos M, Sanromán Á. From waste to resource: valorization of lignocellulosic agri-food residues through engineered hydrochar and biochar for environmental and clean energy applications—a comprehensive review. Foods 2023;12(19):3646.
[54] Tomczyk A, Sokołowska Z, Boguta P. Biochar physicochemical properties: pyrolysis temperature and feedstock kind effects. Rev Environ Sci Biotechnol 2020;19(1):191–215.
[55] Zhang Y, Liang Y, Li S, Yuan Y, Zhang D, Wu Y, Xie H, Brindhadevi K, Pugazhendhi A, Xia C. A review of biomass pyrolysis gas: forming mechanisms, influencing parameters, and product application upgrades. Fuel 2023;347:128461.
[56] Ramos A, Monteiro E, Rouboa A. Biomass pre-treatment techniques for the production of biofuels using thermal conversion methods–a review. Energy Convers Manag 2022;270:116271.
[57] Murtaza G, Ahmed Z, Usman M. Feedstock type, pyrolysis temperature and acid modification effects on physiochemical attributes of biochar and soil quality. Arabian J Geosci 2022;15(3):305.
[58] Qu J, Wang Y, Tian X, Jiang Z, Deng F, Tao Y, Jiang Q, Wang L, Zhang Y. KOH-activated porous biochar with high specific surface area for adsorptive removal of chromium (VI) and naphthalene from water: affecting factors, mechanisms and reusability exploration. J Hazard Mater 2021;401:123292.
[59] Cao X, Chen F, Cen K, Zhang J, Chen D, Li Y. Effect of torrefaction on the pyrolysis behavior, kinetics, and phenolic products of lignin. Biomass Convers Biorefinery 2020:1–9.
[60] Zafeer MK, Menezes RA, Venkatachalam H, Bhat KS. Sugarcane bagasse-based biochar and its potential applications: a review. Emerg Mater 2024;7(1):133–61.
[61] Dhanda A, Raj R, Sathe SM, Dubey BK, Ghangrekar MM. Graphene and biochar-based cathode catalysts for microbial fuel cell: performance evaluation, economic comparison, environmental and future perspectives. Environ Res 2023;231:116143.
[62] Antolini E. Carbon supports for low-temperature fuel cell catalysts. Appl Catal B Environ 2009;88(1–2):1–24.
[63] Zhao H, Zuo H, Wang J, Jiao S. Practical application of graphite in lithium-ion batteries: modification, composite, and sustainable recycling. J Energy Storage 2024;98:113125.
[64] Jin C, Nai J, Sheng O, Yuan H, Zhang W, Tao X, Lou XWD. Biomass-based materials for green lithium secondary batteries. Energy Environ Sci 2021;14(3):1326–79.
[65] Chen X, Li F, Su S, Chen H, Zhang J, Cai D. Efficient honeycomb–shaped biochar anodes for lithium-ion batteries from Eichhornia crassipes biomass. Environ Chem Lett 2021;19(4):3505–10.
[66] Yan P, Ai F, Cao C, Luo Z. Hierarchically porous carbon derived from wheat straw for high rate lithium ion battery anodes. J Mater Sci Mater Electron 2019;30(15):14120–9.
[67] Raza S, Hayat A, Bashir T, Chen C, Shen L, Orooji Y, Lin H. Electrochemistry of 2D-materials for the remediation of environmental pollutants and alternative energy storage/conversion materials and devices, a comprehensive review. Sustain Mater Technol 2024:e00963.
[68] Saletnik B, Zaguła G, Bajcar M, Tarapatskyy M, Bobula G, Puchalski C. Biochar as a multifunctional component of the environment—a review. Appl Sci 2019;9(6):1139.
[69] Liu M, Shi H, Guo L, Fang Z, Chen D, Li W, Deng B, Li W, Du K, Yin H, Wang D. Enhanced graphitization of CO2-derived carbon anodes via Joule heating reformation for high-performance lithium-ion batteries. Carbon 2025;232:119781.
[70] Wang T, Wang Y, Cheng G, Ma C, Liu X, Wang J, Qiao W, Ling L. Catalytic graphitization of anthracite as an anode for lithium-ion batteries. Energy Fuel 2020;34(7):8911–8.
[71] Xing B, Zhang C, Cao Y, Huang G, Liu Q, Zhang C, Chen Z, Yi G, Chen L, Yu J. Preparation of synthetic graphite from bituminous coal as anode materials for high performance lithium-ion batteries. Fuel Process Technol 2018;172:162–71.
[72] Chen G, Jin Y, Zhang Z, Zhao W, Su W, Qing T, Chen J, Li Y. A green phenolic resin/needle coke scrap–based carbon/carbon composite as anode material for lithium-ion batteries. Ionics 2021;27(12):5079–87.
[73] Noel M, Suryanarayanan V. Role of carbon host lattices in Li-ion intercalation/de-intercalation processes. J Power Sources 2002;111(2):193–209.
[74] Yang H, Song B, Ye S, Fang Q, Liu X, Yang Z, Tan X, Zeng G. Reactive species identification in KCl activated biochar/persulfate system under different pH condition: theoretical calculation and column experiments. Chem Eng J 2024;491:151983.
[75] Ayanda OS, Mmuoegbulam AO, Okezie O, Durumin Iya NI, Mohammed SAE, James PH, Muhammad AB, Unimke AA, Alim SA, Yahaya SM, Ojo A. Recent progress in carbon-based nanomaterials: critical review. J Nanoparticle Res 2024;26(5):106.
[76] Zaed MA, Saidur R, Pandey AK, Kadhom M, Tan KH, Cherusseri J, Abdullah N. Utilization of recycled materials for low-cost MXene synthesis and fabrication of graphite/MXene composite for enhanced water desalination performance. Sep Purif Technol 2025;354:129055.
[77] VahidMohammadi A, Rosen J, Gogotsi Y. The world of two-dimensional carbides and nitrides (MXenes). Science 2021;372(6547):eabf1581.

[78] Yong B, Wang Y, Zhu J, Sun S, Ma D, Zhang P. Recent progress on versatile MXene mediated zinc-ion storage technologies. J Energy Storage 2024;93:112334.
[79] Li K, Liang M, Wang H, Wang X, Huang Y, Coelho J, Pinilla S, Zhang Y, Qi F, Nicolosi V, Xu Y. 3D MXene architectures for efficient energy storage and conversion. Adv Funct Mater 2020;30(47):2000842.
[80] Robinson J, Kumari N, Srivastava VK, Taskaeva N, Mohan C. Sustainable and environmental friendly energy materials. Mater Today Proc 2022;69:494–8.
[81] Nagamuthu S, Zhang Y, Xu Y, Sun J, uz Zaman F, Denis DK, Hou L, Yuan C. Non-lithium-based metal ion capacitors: recent advances and perspectives. J Mater Chem A 2022;10(2):357–78.
[82] Vu TT, Le LV, Pham TK, Le TH, Nguyen TH, Thi HPN, Dang TD, La DD. Enhancing li-ion battery anode performance through carbon-coated spherical graphite: influence of synthesis parameters on electrochemical behavior. ChemistrySelect 2025;10(24):e00868.
[83] Kim J, Jeong H, Oh E, Jang J, Lee SW, Kim DH, Han SD, Kim J, Yang J. Negative effect of the calendering process on the interphase formation and electrochemical behavior of reduced graphene oxide electrodes. ACS Appl Mater Interfaces 2024;16(41):56271–84.
[84] Jeong H, Kim J, Lee SH, Kim DU, Kim J, Yang J. Iron-catalyzed graphitization of lignocellulose: a pathway to develop artificial graphite as anode materials for lithium-ion batteries applications. J Alloys Compd 2025;1020:179485.
[85] Liu S, Zhang X, Yan P, Cheng R, Tang Y, Cui M, Wang B, Zhang L, Wang X, Jiang Y, Wang L. Dual bond enhanced multidimensional constructed composite silicon anode for high-performance lithium ion batteries. ACS Nano 2019;13(8):8854–64.
[86] Cheng Z, Wu Y, Huang H. Red phosphorus/graphite composite as a high performance anode for lithium-ion batteries. Solid State Ionics 2023;389:116098.
[87] Dan J, Jin C, Wen L, Xu G, Li X, Sun F, Zhou L, Yue Z. A double-layer-coated graphite anode material for high-rate lithium-ion batteries. Solid State Sci 2023;141:107220.
[88] Ma C, Shi J, Zhao Y, Song NJ, Wang Y. A novel porous reduced microcrystalline graphene oxide supported Fe3O4@ C nanoparticle composite as anode material with excellent lithium storage performances. Chem Eng J 2017;326:507–17.
[89] Zhang H, Hu R, Liu H, Sun W, Lu Z, Liu J, Yang L, Zhang Y, Zhu M. A spherical Sn–Fe 3 O 4@ graphite composite as a long-life and high-rate-capability anode for lithium ion batteries. J Mater Chem A 2016;4(26):10321–8.
[90] Wang L, Zhao Y, Sun J, Li Y, Qu Q, Zheng H. Artificially regulated interphase on natural graphite realizes rapid charge and durable high-temperature cycling of Li-ion batteries. Carbon 2024;230:119656.
[91] Luo J, Wu CE, Su LY, Huang SS, Fang CC, Wu YS, Chou J, Wu NL. A proof-of-concept graphite anode with a lithium dendrite suppressing polymer coating. J Power Sources 2018;406:63–9.
[92] Zou L, Kang F, Li X, Zheng YP, Shen W, Zhang J. Investigations on the modified natural graphite as anode materials in lithium ion battery. J Phys Chem Solid 2008;69(5–6):1265–71.
[93] Ng VMH, Wu S, Liu P, Zhu B, Yu L, Wang C, Huang H, Xu ZJ, Yao Z, Zhou J, Que W. Hierarchical SnO2-graphite nanocomposite anode for lithium-ion batteries through high energy mechanical activation. Electrochim Acta 2017;248:440–8.
[94] Levi MD, Levi EA, Aurbach D. The mechanism of lithium intercalation in graphite film electrodes in aprotic media. Part 2. Potentiostatic intermittent titration and in situ XRD studies of the solid-state ionic diffusion. J Electroanal Chem 1997;421(1–2):89–97.
[95] Ohzuku T, Iwakoshi Y, Sawai K. Formation of lithium-graphite intercalation compounds in nonaqueous electrolytes and their application as a negative electrode for a lithium ion (shuttlecock) cell. J Electrochem Soc 1993;140(9):2490.
[96] Son DK, Kim J, Raj MR, Lee G. Elucidating the structural redox behaviors of nanostructured expanded graphite anodes toward fast-charging and high-performance lithium-ion batteries. Carbon 2021;175:187–201.
[97] Park SM, Salunkhe TT, Yoo JH, Kim IH, Kim IT. Artificial graphite-based silicon composite anodes for lithium-ion batteries. Nanomaterials 2024;14(23):1953.
[98] Wang J, Xia Y, Liu Y, Li W, Zhao D. Mass production of large-pore phosphorus-doped mesoporous carbon for fast-rechargeable lithium-ion batteries. Energy Storage Mater 2019;22:147–53.
[99] Hu D, Chen L, Tian J, Su Y, Li N, Chen G, Hu Y, Dou Y, Chen S, Wu F. Research progress of lithium plating on graphite anode in lithium-ion batteries. Chin J Chem 2021;39(1):165–73.
[100] Petzl M, Danzer MA. Nondestructive detection, characterization, and quantification of lithium plating in commercial lithium-ion batteries. J Power Sources 2014;254:80–7.
[101] Zhao L, Ding B, Qin XY, Wang Z, Lv W, He YB, Yang QH, Kang F. Revisiting the roles of natural graphite in ongoing lithium-ion batteries. Adv Mater 2022;34(18):2106704.
[102] Shi Z, Wang S, Jin Y, Zhao L, Chen S, Yang H, Cui Y, Svanberg R, Tang C, Jiang J, Yang W. Establishment of green graphite industry: graphite from biomass and its various applications. SusMat 2023;3(3):402–15.
[103] Surovtseva D, Crossin E, Pell R, Stamford L. Toward a life cycle inventory for graphite production. J Ind Ecol 2022;26(3):964–79.
[104] Chen S, Liu C, Feng R, Chen Z, Lu Y, Chen L, Huang Q, Guan Y, Yan W, Su Y, Li N. Natural graphite anode for advanced lithium-ion batteries: challenges, progress, and perspectives. Chem Eng J 2025;503:158116.
[105] Jiang J, Liu J, Chen Y, Sun R, Liu Y, Yang Y, Yang Y, Yang G. Preparation of hierarchical hexagonal nanoplates NiO composite with microcrystalline graphite for highly reversible lithium storage. J Alloys Compd 2020;815:152333.
[106] Jiang J, Ma C, Yang Y, Ding J, Ji H, Shi S, Yang G. Synergetic interface between NiO/Ni3S2 nanosheets and carbon nanofiber as binder-free anode for highly reversible lithium storage. Appl Surf Sci 2018;441:232–8.
[107] Ju Z, Guo C, Qian Y, Tang B, Xiong S. Direct large-scale synthesis of 3D hierarchical mesoporous NiO microspheres as high-performance anode materials for lithium ion batteries. Nanoscale 2014;6(6):3268–73.
[108] Sun J, Zheng G, Lee HW, Liu N, Wang H, Yao H, Yang W, Cui Y. Formation of stable phosphorus–carbon bond for enhanced performance in black phosphorus nanoparticle–graphite composite battery anodes. Nano Lett 2014;14(8):4573–80.
[109] Yang M, Dai J, He M, Duan T, Yao W. Biomass-derived carbon from Ganoderma lucidum spore as a promising anode material for rapid potassium-ion storage. J Colloid Interface Sci 2020;567:256–63.
[110] Deng Q, Liu H, Zhou Y, Luo Z, Wang Y, Zhao Z, Yang R. N-doped three-dimensional porous carbon materials derived from bagasse biomass as an anode material for K-ion batteries. J Electroanal Chem 2021;899:115668.
[111] Wu G, Zhang H, Zhang X, Guan Q, Zhang W, Lu J, Lan W, Li Z, Yang S, Shi H. Converting biomass tar into N-doped biochar: a promising anode material for enhanced sodium-ion batteries. J Anal Appl Pyrolysis 2025;188:107051.
[112] Jiménez-Pérez R, González-Sanchez MI, Gomis-Berenguer A, Iniesta J, Valero E. Enhanced surface properties and electrochemical performance of carbon-based screen-printed electrodes via hydrogen peroxide activation. Electrochim Acta 2025:146721.
[113] Gao L, Ma J, Li S, Liu D, Xu D, Cai J, Chen L, Xie J, Zhang L. 2D ultrathin carbon nanosheets with rich N/O content constructed by stripping bulk chitin for high-performance sodium ion batteries. Nanoscale 2019;11(26):12626–36.
[114] Sapnik AF, Bechis I, Collins SM, Johnstone DN, Divitini G, Smith AJ, Chater PA, Addicoat MA, Johnson T, Keen DA, Jelfs KE. Mixed hierarchical local structure in a disordered metal–organic framework. Nat Commun 2021;12(1):2062.
[115] Bechis I, Sapnik AF, Tarzia A, Wolpert EH, Addicoat MA, Keen DA, Bennett TD, Jelfs KE. Modeling the effect of defects and disorder in amorphous metal–organic frameworks. Chem Mater 2022;34(20):9042–54.
[116] Saleh HM, Hassan AI. Synthesis and characterization of nanomaterials for application in cost-effective electrochemical devices. Sustainability 2023;15(14):10891.
[117] Cowlard FC, Lewis JC. Vitreous carbon—A new form of carbon. J Mater Sci 1967;2:507–12.
[118] Adams RA, Varma A, Pol VG. Carbon anodes for nonaqueous alkali metal-ion batteries and their thermal safety aspects. Adv Energy Mater 2019;9(35):1900550.
[119] Dresselhaus MS, Dresselhaus G. Intercalation compounds of graphite. Adv Phys 2002;51(1):1–186.
[120] Xie L, Tang C, Bi Z, Song M, Fan Y, Yan C, Li X, Su F, Zhang Q, Chen C. Hard carbon anodes for next-generation Li-ion batteries: review and perspective. Adv Energy Mater 2021;11(38):2101650.
[121] Wang Y, Abrego-Martinez JC, Quéméré S, Vanpeene V, Roué L. Scalable spray-dried graphite/CNT/silicon composites with enhanced cycling stability for Li-ion battery anodes. Energy Mater 2026;6(2):N–A.
[122] Dong H, Hou J, Ma Y, Xin J, Wei M, Li S. Dual carbon-network armored silicon anode: graphene-CNT reinforced pomegranate architecture enabling long-cycle lithium-ion battery. J Energy Storage 2025;132:117726.
[123] Hu M, Wu H, Zhang GJ. High-performance silicon/graphite anode prepared by CVD using SiCl4 as precursor for Li-ion batteries. Chem Phys Lett 2023;833:140917.
[124] Hao Y, Yang X, Gao Y, Saleem MH, Li J, Wu C, Liu G. High-toughness design of micron-sized silicon/carbon composite as practical anode for lithium-ion batteries. Chem Eng J 2025;515:163258.
[125] Nowak AP. Composites of tin oxide and different carbonaceous materials as negative electrodes in lithium-ion batteries. J Solid State Electrochem 2018;22(8):2297–304.
[126] He C, Wu S, Zhao N, Shi C, Liu E, Li J. Carbon-encapsulated Fe3O4 nanoparticles as a high-rate lithium ion battery anode material. ACS Nano 2013;7(5):4459–69.
[127] Sethuraman VA, Hardwick LJ, Srinivasan V, Kostecki R. Surface structural disordering in graphite upon lithium intercalation/deintercalation. J Power Sources 2010;195(11):3655–60.
[128] Sandhu ZA, Raza MA, Aman F, Arshid MS, Jaffary SDK, Arshad S, Raza M, Al-Sehemi AG, DEGE N. Graphene-metal oxide nanocomposites: empowering next-generation energy storage devices. Mater Sci Eng, B 2025;313:117947.
[129] Kausar A, Ahmad I. Energy systems endorsing graphene nanocomposites—Next energy vision. Next Energy 2024;4:100148.
[130] Chaudhuri A, Chaudhuri A, Joydhar A. Graphene nanocomposites and applications in electrochemical energy storage materials. Mater Today Proc 2022;64:1569–81.
[131] Chrisma RB, Jafri RI, Anila EI. A review on the electrochemical behavior of graphene–transition metal oxide nanocomposites for energy storage applications. J Mater Sci 2023;58(14):6124–50.
[132] Gautam S, Rialach S, Paul S, Goyal N. MOF/graphene oxide based composites in smart supercapacitors: a comprehensive review on the electrochemical evaluation and material development for advanced energy storage devices. RSC Adv 2024;14(20):14311–39.
[133] Pour GB, Ashourifar H, Aval LF, Solaymani S. CNTs-supercapacitors: a review of electrode nanocomposites based on CNTs, graphene, metals, and polymers. Symmetry 2023;15(6):1179.
[134] Vinodhini SP, Xavier JR. Recent progress in graphene-based nanocomposites for enhanced energy storage and corrosion protection. J Mater Sci 2025;60(34):14837–79.

[135] Wang JR, Yang DH, Xu YJ, Hou XL, Ang EH, Wang DZ, Zhang L, Zhu ZD, Feng XY, Song XH, Xiang HF. Recent developments and the future of the recycling of spent graphite for energy storage applications. N Carbon Mater 2023;38(5):787–803.
[136] Liang Y, Zhang W, Wu D, Ni QQ, Zhang MQ. Interface engineering of carbon-based nanocomposites for advanced electrochemical energy storage. Adv Mater Interfac 2018;5(14):1800430.
[137] Tarascon JM, Armand M. Issues and challenges facing rechargeable lithium batteries. Nature 2001;414(6861):359–67.
[138] Nitta N, Wu F, Lee JT, Yushin G. Li-ion battery materials: present and future. Mater Today 2015;18(5):252–64.
[139] Poizot PLSG, Laruelle S, Grugeon S, Dupont L, Tarascon JM. Nano-sized transition-metal oxides as negative-electrode materials for lithium-ion batteries. Nature 2000;407(6803):496–9.
[140] Cabana J, Monconduit L, Larcher D, Palacin MR. Beyond intercalation-based Li-ion batteries: the state of the art and challenges of electrode materials reacting through conversion reactions. Adv Mater 2010;22(35):E170–92.
[141] Obrovac MN, Chevrier VL. Alloy negative electrodes for Li-ion batteries. Chem Rev 2014;114(23):11444–502.
[142] Li JY, Xu Q, Li G, Yin YX, Wan LJ, Guo YG. Research progress regarding Si-based anode materials towards practical application in high energy density Li-ion batteries. Mater Chem Front 2017;1(9):1691–708.
[143] Stevens DA, Dahn JR. The mechanisms of lithium and sodium insertion in carbon materials. J Electrochem Soc 2001;148(8):A803–11.
[144] Slater MD, Kim D, Lee E, Johnson CS. Sodium-ion batteries. Adv Funct Mater 2013;23(8):947–58.
[145] Ao L, Wu C, Wang X, Xu Y, Jiang K, Shang L, Li Y, Zhang J, Hu Z, Chu J. Superior and reversible lithium storage of SnO2/graphene composites by silicon doping and carbon sealing. ACS Appl Mater Interfaces 2020;12(18):20824–37.
[146] Wu Z, Dong J, Li X, Zhao X, Ji C, Zhang Q. Interlayer decoration of expanded graphite by polyimide resins for preparing highly thermally conductive composites with superior electromagnetic shielding performance. Carbon 2022;198:1–10.
[147] Naguib M, Mochalin VN, Barsoum MW, Gogotsi Y. 25th anniversary article: MXenes: a new family of two-dimensional materials. Adv Mater 2014;26(7):992–1005.
[148] Zhang C, Anasori B, Seral-Ascaso A, Park SH, McEvoy N, Shmeliov A, Duesberg GS, Coleman JN, Gogotsi Y, Nicolosi V. Transparent, flexible, and conductive 2D titanium carbide (MXene) films with high volumetric capacitance. Adv Mater 2017;29(36):1702678.
[149] Xu Y, Zhang C, Zhou M, Fu Q, Zhao C, Wu M, Lei Y. Highly nitrogen doped carbon nanofibers with superior rate capability and cyclability for potassium ion batteries. Nat Commun 2018;9(1):1720.
[150] Gao Y, Yu Q, Yang H, Zhang J, Wang W. The enormous potential of sodium/potassium-ion batteries as the mainstream energy storage technology for large-scale commercial applications. Adv Mater 2024;36(39):2405989.

Further Reading

[1] Nair AS, Sreejakumari SS, Venkatesan J, Rakhi RB, Sumathi RR, Jayasankar K. A novel top-down approach for high yield production of graphene from natural graphite and its supercapacitor applications. Diam Relat Mater 2024;144:111025.